



UNIVERSITY OF LEEDS

This is a repository copy of *Low-temperature densification of Mg-doped hydroxyapatite fine powders under hydrothermal hot processing conditions*.

White Rose Research Online URL for this paper:
<http://eprints.whiterose.ac.uk/117521/>

Version: Accepted Version

Article:

Montoya-Cisneros, KL, Rendón-Angeles, JC, Matamoros-Veloza, Z et al. (2 more authors) (2017) Low-temperature densification of Mg-doped hydroxyapatite fine powders under hydrothermal hot processing conditions. *Ceramics International*, 43 (15). pp. 11907-11919. ISSN 0272-8842

<https://doi.org/10.1016/j.ceramint.2017.06.039>

© 2017 Elsevier Ltd and Techna Group S.r.l. This manuscript version is made available under the CC-BY-NC-ND 4.0 license <http://creativecommons.org/licenses/by-nc-nd/4.0/>

Reuse

Items deposited in White Rose Research Online are protected by copyright, with all rights reserved unless indicated otherwise. They may be downloaded and/or printed for private study, or other acts as permitted by national copyright laws. The publisher or other rights holders may allow further reproduction and re-use of the full text version. This is indicated by the licence information on the White Rose Research Online record for the item.

Takedown

If you consider content in White Rose Research Online to be in breach of UK law, please notify us by emailing eprints@whiterose.ac.uk including the URL of the record and the reason for the withdrawal request.

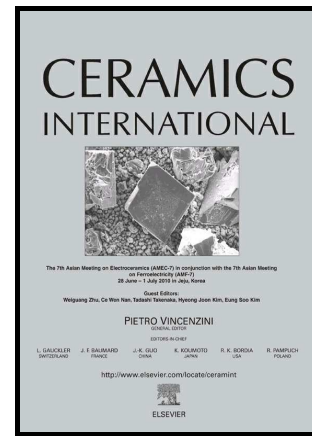


eprints@whiterose.ac.uk
<https://eprints.whiterose.ac.uk/>

Author's Accepted Manuscript

Low-temperature densification of Mg-doped hydroxyapatite fine powders under hydrothermal hot processing conditions

K.L. Montoya-Cisneros, J.C. Rendón-Angeles, Z. Matamoros-Veloza, A. Matamoros-Veloza, K. Yanagisawa



www.elsevier.com/locate/ceri

PII: S0272-8842(17)31241-5
DOI: <http://dx.doi.org/10.1016/j.ceramint.2017.06.039>
Reference: CERI15561

To appear in: *Ceramics International*

Received date: 4 June 2016
Revised date: 5 June 2017
Accepted date: 6 June 2017

Cite this article as: K.L. Montoya-Cisneros, J.C. Rendón-Angeles, Z. Matamoros-Veloza, A. Matamoros-Veloza and K. Yanagisawa, Low-temperature densification of Mg-doped hydroxyapatite fine powders under hydrothermal hot processing conditions, *Ceramics International*, <http://dx.doi.org/10.1016/j.ceramint.2017.06.039>

This is a PDF file of an unedited manuscript that has been accepted for publication. As a service to our customers we are providing this early version of the manuscript. The manuscript will undergo copyediting, typesetting, and a review of the resulting galley proof before it is published in its final citable form. Please note that during the production process errors may be discovered which could affect the content, and all legal disclaimers that apply to the journal pertain

Low-temperature densification of Mg-doped hydroxyapatite fine powders under hydrothermal hot processing conditions

K.L. Montoya-Cisneros^a, J.C. Rendón-Angeles^{a,*}, Z. Matamoros-Veloza^b, A. Matamoros-Veloza^c, K. Yanagisawa^d.

^aResearch Institute of Advanced Studies of the National Polytechnic Institute, Saltillo Campus, Ramos Arizpe, 25900, Coahuila Mexico.

^bTechnological Institute of Saltillo, Faculty of Metal-Mechanics, Saltillo, 25280, Coahuila, Mexico.

^cInstitute of Thermofluids, School of Mechanical Engineering, University of Leeds, Leeds LS2 9JT, United Kingdom.

^dResearch Laboratory of Hydrothermal Chemistry, Faculty of Science, Kochi University. Kochi 780-8073, Japan.

*Corresponding author: Ceramic Engineering Department Av. Industria Metalúrgica No. 1062, Parque Industrial Saltillo-Ramos Arizpe Ramos Arizpe 25900, Coahuila, Mexico. Tel. +52-844-438-9600; Fax: +52-844-438-9610. jcarlos.rendon@cinvestav.edu.mx

Abstract:

Densification of calcium hydroxyapatite fine powders doped with different concentrations of Mg (2, 4 and 6 mol % Mg, MgHA) was successfully achieved for the first time in a nearly fully dense state using the

hydrothermal hot pressing (HHP) technique at low temperatures. Consolidation of MgHA powders was studied under different temperatures (150–240 °C), reaction times (1–6 h), and powder particle size (20 nm–1.5 µm). X-Ray diffraction analyses indicated that the particle densification under HHP conditions proceeded without any variation in the crystalline structure and regardless of the Mg content. The results from this work showed that an increase in temperature accelerates the reaction between MgHA particles and water (solvent) mixed during the hydrothermal treatment. Particle packing associated with bulk densification was achieved through a massive dissolution-recrystallisation mechanism, which induced the formation of small particles that rapidly crystallised on the surface of the partially dissolved original MgHA particles. The optimum conditions to obtain pellets with a high apparent density of $3.0758 \pm 0.001 \text{ g/cm}^3$ and tensile strength value of $12.6 \pm 0.6 \text{ MPa}$ were 10 wt% of water at a temperature of 240 °C with a 6 h reaction time and 6 mol % of Mg (MgHA3). The use of the HHP technique coupled with the fine particle size and reactivity of the MgHA precursor powders with water allowed us to produce disks that were compacted to a nearly full dense state with a low content of open porosity of 2.0 %.

Keywords:

Hydroxyapatite, Hydrothermal hot-pressing, Low-temperature densification, Tensile strength, Magnesium.

1. Introduction

Bioceramic materials based on hydroxyapatite (HA) are important for the development of human tissue implants because their chemical compositions ($A_{10}(BO_4)_6(X)_2$) are comparable to those of bone and soft human tissues as well as because they have high biocompatibility, bioactivity and osteoconductivity [1,2]. The incorporation of ions at various concentrations in the hexagonal structure (i.e., A, B or X sites) of HA determines its crystallinity and non-stoichiometry. Ionic substitutions (e.g., Mg^{2+} , Zn^{2+} , Sr^{2+} , Si^{4+} and Mn^{2+}) in

the HA structure have been reported to improve the biological performance of calcium phosphate phases, thereby enhancing osseointegration, mechanical strength and implantation efficiency [3,4]. Furthermore, changes in the chemical composition of HA influence its physical, chemical and physiological properties, which consequently have an effect on biomineralisation processes, bioactivity enhancement, and ion delivery for treating bone diseases [3,4]. Mg is present in the human body at concentrations between 1 and 6 mol %, and half of this amount is found in hard tissues. This element plays an important role in hard tissue metabolism, influencing osteoblast and osteoclast activity, and as a result, controlling the growth of bone [5-11]. In vivo studies have demonstrated that the presence of Mg in HA improves cell behaviour, adhesion with synthetic hard tissues, proliferation, and metabolic activation [12]. For these reasons, Mg is an interesting element to study regarding its possible ionic substitutions into the HA structure [3,13-15].

Densification of HA ceramic powders has been widely investigated for the production of highly dense or porous specimens. Various factors influence the densification process of powder materials during the sintering stage. One of the most important factors is the particle packing of the green pellet, which depends on the particle morphology and size [16,17]. Previous studies have investigated the preparation of highly packed structures to obtain dense and controlled porous HA monolithic specimens for different potential applications using the hydrothermal hot pressing (HHP) technique. Dense specimens with high mechanical strength can be obtained under continuous loading at low temperatures (150–300 °C), which is achieved according to interactions between the particles and water (used as the solvent medium) [18-25]. Over the last two decades, several researchers have studied the densification of pure HA powders under HHP conditions. Some studies have focused on the selection of the solvent medium and its concentration to obtain in-situ crystallisation of elongated submicron-sized HA crystals using mixtures of $\text{Ca}(\text{OH})_2$ with either dibasic calcium phosphate dihydrate (DCPD) [19] or octacalcium phosphate (OCP) [26] as precursors. Few studies have reported that after reacting these compounds with water and ammonia solutions, HA crystals grow perpendicularly in the direction of the applied loading pressure, producing a dense lamellar microstructure with high tensile strength [19,27]. Recently, the chemical reactivity of pure and calcium deficient submicron-sized HA powders with water under HHP conditions was examined using 10 to 20 wt% of water, temperatures between 100 and 200

°C, and loading pressures between 15 and 60 MPa for reaction intervals between 12 and 24 h [20].

Densification of these powders was achieved by a coupled process involving the partial dissolution of the HA powder and simultaneous crystallisation of the dissolved species in water [20]. This process caused sufficient particle packing to produce compact structures with relative apparent densities of over 90 %. An alternative processing route to obtain denser HA monolithic specimens has recently been proposed. This method involves HA powder densification at low temperatures (200 °C) by HHP and a subsequent sintering treatment conducted at high temperature [22]. Hence, hydrothermal hot-pressing has proved to be effective for producing dense pellets by accelerating the sintering kinetics and therefore constitutes an emerging new processing route for the production of high-density bioceramic materials [22].

In recent years, many efforts have been made to improve the densification of HA particles [18-25,27]. However, a literature survey suggests that the compaction process of calcium hydroxyapatite powders partially doped with Mg has not been carried out using the hydrothermal hot-pressing technique at relatively low temperatures. Therefore, the present study is the first attempt to produce compaction with MgHA fine powders to the nearly full dense state under HHP conditions using water as the solvent medium. Preliminary attempts were conducted to provide details on the reactivity of the MgHA powders with water to optimise the experimental HHP conditions (water content, temperature and reaction time), to achieved sufficient particle packing and obtain compacts with relative apparent density values higher than 85 %. Additionally, the effect of the particle size and content of Mg on the HHP densification stage of the MgHA particles was evaluated by the Archimedes principle, using a helium gas pycnometer, while the MgHA pellets densification pathway was investigated by Hg intrusion porosimetry. The powder packing promoted by the reactivity of MgHA particles with water was correlated with the mechanical properties of the hydrothermal hot pressed (HHP'ed) dense specimens. The disk tensile strength was evaluated using the Brazilian test.

2. Experimental

2.1 Preparation of MgHA precursor powders

Preparation of precursor powders corresponding to MgHA solid solutions of $\text{Ca}_{10-x}\text{Mg}_x(\text{PO}_4)_6\text{OH}_2$, with an x content of 2, 4 and 6 mol % Mg, were synthesised by hydrothermal microwave-assisted treatments. Initially, precursor gels were coprecipitated by mixing stoichiometric contents of calcium nitrate, magnesium nitrate and diammonium hydrogen phosphate ($\text{Ca}(\text{NO}_3)_2 \cdot 4\text{H}_2\text{O}$, $\text{Mg}(\text{NO}_3)_2 \cdot 6\text{H}_2\text{O}$, $(\text{NH}_4)_2\text{HPO}_4$, Sigma-Aldrich, 99 % purity) to maintain a molar Ca+Mg/P ratio of 1.67. In a different set of experiments, a precursor gel containing 6 mol % of Mg was prepared using sodium tripolyphosphate as the phosphate source, while 2-propanol was used as a pH controlling medium [28]. A volume of 50 ml of each colloidal suspension was transferred to a double-walled Teflon high pressure vessel and placed in a microwave instrument (MARS-5X, CEM Corp, USA) that was operated at a power of 1200 W. MgHA particle crystallisation was carried out at 150 °C for 1 h under autogenous pressure. The reaction products obtained were washed and freeze-dried (-47 °C, 3 MPa) using a Labconco Freeze Dryer. X-Ray powder diffraction (XRD) analyses indicated that all of the prepared powders could be indexed with the hexagonal crystalline structure of HA (JCPDS card No. 09-0432). However, a slight displacement of the diffraction peaks was observed for MgHA powders, which is consistent with the gradual incorporation of Mg into the hexagonal structure of HA (Fig. 1a). Similarly, slight differences in the MgHA powder particle sizes were observed as a function of the Mg content. Other powder features, such as the surface area and chemical composition of the precursor, are summarised in Table 1. The original morphology of the MgHA particles was determined by transmission electron microscopy (TEM) observations and the images are shown in Figs. 1(b-d).

2.2 Densification of MgHA powders under HHP conditions

A MgHA powder sample of 3.5 g was carefully kneaded in a mortar with various quantities of deionised water (10–20 wt%). The moistened powder was then placed in a cylindrical autoclave chamber (20 mm in diameter), which is used in conventional HHP, which is described in ref. [29]. The HHP autoclave was subsequently loaded at a constant pressure of 60 MPa, and this pressure was continuously applied during the heating, compaction time and cooling-down stages. All of the HHP treatments were carried out at a constant

heating rate of 10 °C/min up to the desired temperature, which varied between 150 and 240 °C. Powder densification was conducted for several reaction times from 1 to 6 h. After the hydrothermal treatment, the vessel was rapidly cooled to room temperature using an electric fan, and the compact disk (approximately 5 mm thick and 20 mm diameter) was then carefully removed to avoid damage or fracturing. All of the pellets were polished and dried at 80 °C overnight in an oven.

2.3 Characterisation

X-Ray diffraction analyses were conducted to identify the crystalline phases in the compacted pellets. Diffraction patterns were collected from 10 to 80° 2 θ at a scanning speed of 4 °/min and 0.02° step in 2 θ / θ scanning mode using a X-ray diffractometer (Rigaku Ultima IV, Japan) equipped with Cu K α radiation ($\alpha = 1.54056 \text{ \AA}$) at 40 kV and 20 mA. The microstructure of the compacts disks was observed using scanning electron microscopy (JEOL 6500 FE-SEM, Japan) on fractured specimen surfaces after the mechanical testing. The variation on the vibrational intensity of the OH⁻ and PO₄³⁻ functional groups during the MgHA powder HHP densification stage was evaluated by Fourier transform infrared spectroscopy (FT-IR, JASCO 4000, Japan) analyses. The chemical composition of the pellets was determined by chemical analysis using inductively coupled plasma atomic emission spectrometry (ICP-AES, Shimadzu Multi-type ICP Emission Spectrometer ICP-9000, Japan).

The tensile strength of all of the pellets was measured by the Brazilian test, which is commonly used for brittle materials [30,31]. In this test, the disk-shaped pellet was placed between jaws with a curvature radius of 10 cm. Then, diametral compression was applied using a universal testing machine (Autograph AG-IS Shimadzu 50 KN, Japan). The test was conducted at a constant crosshead speed of 0.5 mm/min until fracture of the specimen occurred in parallel with the loading diametral plane. The tensile strength was calculated using Eq. 1, where P_F is the maximum load, d is the diameter of the pellet and t is the thickness of the sample.

$$\sigma_f = \frac{2PF}{\pi dt} \quad (1)$$

The apparent density was determined by means of the Archimedes method by placing the sample in boiling water for 12 h [32]. For comparison purposes, the apparent density of all MgHA compacts was carried out using a helium pycnometer (Multipycnometer Quantachrome, USA). Prior to the density measurements, calibration of the pycnometer was carried out using a standard stainless steel sphere with a volume of 56.5592 cm³, which was located inside the measuring cell (volume 135 cm³). The MgHA compacts were previously weighed, and their volume was measured four times at a helium pressure of 0.117 MPa and the average apparent density value was calculated for each sample. Furthermore, the pore volume and pore size distribution were determined by mercury intrusion porosimetry (MIP) analyses using a Micromeritics AutoPore IV 9500, Japan. Moreover, three green pellets were prepared using 1.0 g of the fine particle size MgHA powders containing 2 and 6 mol % Mg. The disks obtained at a uniaxial pressing of 60 MPa without water were then characterised by mercury intrusion porosimetry to determine the pore size and distribution inside the pellets before the HHP treatment.

3. Results and Discussion

3.1 Structural aspects of MgHA pellets prepared under hydrothermal hot pressing conditions

HHP densification of MgHA fine powders containing 2, 4, and 6 mol % Mg, was conducted at a low temperature using only water. The purpose of the experiments was to evaluate the feasibility of solidifying MgHA compacts according to the chemical reaction between the MgHA particles and water under HHP conditions. The relevant experimental conditions, together with the chemical and physical properties of the compacted MgHA pellets, are summarised in Table 2. The results indicate that the densification temperature was the most important parameter for the rapid densification of MgHA powders, contrary not the reaction time or water content, which both had no effect. Controlling the temperature led to highly dense MgHA pellets with an apparent density up to 3.0758 ± 0.001 g/cm³, near the theoretical density value of the HA

(3.156 g/cm³). This dense specimen was obtained at 240 °C after 6 h using a water content of 10 wt%. In all runs after the compaction treatment, the chemical composition of the specimen relative to the Mg content did not vary markedly, as confirmed by the X-ray diffraction patterns (Fig. 2) and wet chemical analyses (Table 2).

XRD analyses were conducted to study the structural phase changes of the raw MgHA compounds and the formation of reaction by-products. Typical XRD patterns of MgHA pellets containing different Mg contents (2, 4 and 6 mol % Mg), which were prepared under HHP conditions at 200 °C for 6 h using a water content of 10 wt% and a constant loading pressure of 60 MPa, are shown in Fig. 2. In general, the diffraction patterns of all of the compacted pellets were indexed with the pattern of the pure HA crystalline phase, which has a hexagonal structure (space group P6₃/m, JCPDS card No. 09-0432). In all of the cases studied, XRD analyses confirmed that no remarkable structural differences occurred during the hydrothermal densification stage because the MgHA pellets had poor crystallinity, which was consistent with the results for all of the raw MgHA particles used (Figs. 2a-c). Additionally, the formation of calcium phosphate secondary phases, i.e., monetite (CaHPO₄), did not take place during the HHP densification stage; this was confirmed by the powder XRD patterns, which did not reveal the presence of monetite at a 2θ angle of 30.1°. A similar behaviour was also observed for the MgHA4 (6 mol % Mg) powders that were prepared with Na₅P₃O₁₀ although these powders have a larger particle size (1.5 μm) and higher crystallinity in comparison to those prepared using the (NH₄)₂HPO₄ precursor (Fig. 1a). From the structural analyses, water used as the solvent did not significantly alter the structure of MgHA powders compacted under HHP conditions.

The FT-IR spectra of MgHA3 pellets (6 mol % Mg) compacted for 6 h using 10 wt% of water at different temperatures are shown in Fig. 3. In general, all of the vibrational bands found in the spectra correspond to the main functional groups of PO₄³⁻ and were assigned to the symmetric stretching mode of P-O (ν₁ at 966 cm⁻¹), bending modes of O-P-O (ν₂ at 471 cm⁻¹ and ν₄ at 565 and 602 cm⁻¹), and the antisymmetric stretching mode of P-O (ν₃ at 1041 and 1093 cm⁻¹). The peaks related to the vibrational modes for the OH⁻ group were determined at 3570 cm⁻¹ (ν_S, stretching) and 636 cm⁻¹ (ν_L, librational) [33]. However, a broad band in the

wavenumber range of 3200–3600 cm^{-1} , corresponding to water molecules, formed during the HHP densification treatment. These water molecules were adsorbed on the surface of the packed MgHA particles inside the pellet [34]. No particular differences in the content of water adsorbed at different reaction temperatures was determined by the FT-IR analyses, indicating that the nominal water (10 wt%) kneaded with the MgHA powder reacted completely and a layer of solvated water molecules was produced on the surface of the packed particles under HHP conditions. The presence of water molecules did not cause significant structural variations, as is supported by the XRD analyses (Fig. 2).

3.2 Low-temperature densification of MgHA powders by HHP

MgHA powder densification was evaluated by measuring the apparent density of the MgHA compacts using a gas helium pycnometer. These data together with the open porosity calculated on all of the pellets are included in Table 2. Fig. 4 shows the variation of apparent density of all of the pellets produced from MgHA powders obtained by the hydrothermal microwave-assisted process. In addition, the effect of the particle size as well as the nominal composition of Mg (2–6 mol %) of the powder are also included in Fig. 4, as both parameters might affect the hydrothermal reaction between water and the particles, which dominates the particle packing process under continuous compaction. The experimental parameters, such as the temperature, time of reaction, and water content, were all evaluated according to the densification behaviour of the MgHA powder precursors. All of the HHP treatments were conducted at the selected standard loading pressure of 60 MPa.

In general, these results indicate that the water content used to moisten the MgHA powder precursor had no effect on the densification process (Fig. 4a). In all cases, the apparent density of the pellets remained constant, with no significant increments after the HHP treatment was carried out with three different amounts of water under the selected standard conditions of 200 °C for 6 h. In agreement with these results, a water content of 10 wt% was sufficient to react fully with the particles and achieve a high densification for the

MgHA3 and MgHA4 powders, which contained 6 mol % Mg in comparison with the fine MgHA particles, which had a low content of Mg (2 mol % MgHA1 and 4 mol % MgHA2). A water content above 15 wt% caused moisture leakage from the pellet during the heating and compaction stages. The leaked moisture migrated to the inner piston reservoir volume and was then condensed during the cooling stage of the HHP treatment [29]. This excess water content did not react with the MgHA particles and therefore had a limited contribution to the densification process of the powders. Thus, the apparent density of the MgHA3 and MgHA4 compacts remained almost constant when a water contents above 15 wt% was used for the densification process (Fig. 4a). Furthermore, the variation of the apparent density of the pellets produced over various intervals during the reaction under HHP standard conditions (200 °C with 10 wt% of water) is shown in Fig. 4b. These results indicate that increasing the reaction time over 1 h led to a continuous enhancement of the densification of the MgHA3 (20 nm particle size) and MgHA4 (1.5 μm particle size) powders regardless of the particle size, and this process gradually proceeded to the longest selected reaction time of 6 h. Nevertheless, the apparent density values of the MgHA4 pellets were somewhat lower ($2.9844 \pm 0.018 \text{ g/cm}^3$) than the apparent density values achieved at higher temperatures ($3.0425 \pm 0.024 \text{ g/cm}^3$, 240 °C, Table 2). By contrast, powders containing 2 (MgHA1, ▲) and 4 (MgHA2, ■) mol % Mg with fine particle sizes (39 and 32 nm) did not exhibit a systematic increase in their apparent density by increasing the reaction time to 6 h. These particles are chemically more stable than particles containing 6 mol % Mg. These powders exhibited only a slight reactivity with water under HHP conditions that reached average apparent density values of 2.9564 and 2.9544 g/cm^3 . Therefore, based on our results, a large content of Mg (6 mol %) significantly improves the particle reactivity with water under HHP conditions enhancing the MgHA particle packing to high apparent densities. Moreover, the difference in the apparent density values between the MgHA3 and MgHA4 pellets compacted with different water contents and for several reaction intervals is attributed to the precursor particle size. Although the micron-sized (1.5 μm average size) MgHA4 particles underwent a marked densification from the green pellet stage, these particles exhibited only a slightly increase in their apparent density and reached a maximum value of $3.0140 \pm 0.020 \text{ g/cm}^3$ when they were compacted with 20 wt% water at 200 °C for 6 h.

Alternatively, the results indicate that all of the precursor MgHA powders were rapidly densified, irrespective of the reaction temperature under the HHP conditions investigated (6 h, 10 wt% of water, see Fig. 4c). The maximum value of the apparent density ($3.0758 \pm 0.001 \text{ g/cm}^3$) achieved at $240 \text{ }^\circ\text{C}$ was determined for the MgHA3 powder (6 mol % Mg) which had the smallest particle size of 20 nm. Furthermore, marginal decreases in the apparent density to values of $2.9815 \pm 0.004 \text{ g/cm}^3$ and $2.9651 \pm 0.042 \text{ g/cm}^3$ were obtained, when the pellets were densified using MgHA2 (4 mol % Mg, mean particle size of 32 nm) and MgHA1 (2 mol % Mg, mean particle size of 39 nm), respectively. Although the powder densification process might be affected by the nominal particle size of the MgHA powder precursors, the results indicated that the nominal particle size did not hinder the densification process during the HHP treatment as high apparent density values over $2.9637 \pm 0.035 \text{ g/cm}^3$ were obtained by $1.5 \text{ }\mu\text{m}$ precursors (MgHA4, 6 mol % Mg), even at temperatures over $150 \text{ }^\circ\text{C}$. In addition, all of the MgHA pellets obtained at the lowest temperature ($150 \text{ }^\circ\text{C}$), which were prepared using MgHA powder precursors with a particle size below 40 nm, had apparent densities of up to $3.0339 \pm 0.009 \text{ g/cm}^3$. Moreover, at $150 \text{ }^\circ\text{C}$, MgHA4 particles with an average size of $1.5 \text{ }\mu\text{m}$, remarkably reacted with water, but the pellet produced had a low particle cohesion because it was broken down during the apparent density measurement in boiling water.

Overall, the factors that strongly influence the densification of MgHA powders are the reaction temperature, Mg content and particle size, rather than the reaction time and water content. The increase in the apparent density of the MgHA pellet with temperature is likely due to an increase in the speed of the dissolution-recrystallisation reaction mechanism, and, it is also greatly improved by the larger surface area of the MgHA precursors, which is associated with their particle size, making them more reactive in water under hydrothermal conditions. This inference is supported by the submicron-sized MgHA4 particles, which had the lowest surface area, rapidly reacting at relatively low temperatures ($240 \text{ }^\circ\text{C}$) to produce pellets with a high apparent density ($3.0425 \pm 0.024 \text{ g/cm}^3$).

3.3 Packing mechanism of MgHA powders under HHP conditions

The mechanism associated with particle densification during the HHP process was investigated via systematic mercury intrusion porosimetry measurements. The densification results illustrate that the reaction temperature is the most important parameter for enhancing the reaction kinetics between MgHA particles with water during HHP powder consolidation. Hence, the particle packing mechanism associated with bulk MgHA powder densification has been investigated with the aim of determining the effects of the reaction temperature, particle size and Mg concentration.

Fig. 5 shows representative cumulative mercury intrusion curves as a function of the pore size, and these results also include the curve corresponding to the green pellets prepared MgHA1 (Fig. 5a), MgHA3 (Fig. 5b) and MgHA4 powders (Fig. 5c) [35]. These curves provide evidence of the total content of mercury intruded into the open porosity remaining on the HHP specimens. In general, the MgHA1 and MgHA3 cumulative curves analysed showed a similar behaviour, although, the MgHA1 green pellet has a broad range of pore sizes, which vary between 0.006 – 0.8 μm . This sample contains a large amount of porosity with sizes below 0.052 μm . Pores with a size below 0.006 μm in diameter were detected by mercury intrusion analysis (as shown in Fig. 5a). The total mercury volume intruded into the green pellet was 0.3423 mL/g, and this value corresponds to the total open porosity of the green pellet. The volume of mercury intrusion was reduced a 52.0 % when the pellets underwent the HHP treatment even at the lowest treatment temperature of 150 $^{\circ}\text{C}$. The reduction in the open porosity observed in the pellet produced at low temperature (150 $^{\circ}\text{C}$) is likely initiated by the reaction of the MgHA particles with water under the hydrothermal conditions. The maximum reduction of 57.0 %, which corresponds to open porosity closure, was obtained at reaction temperatures above 200 $^{\circ}\text{C}$. By contrast, the MgHA3 green pellet containing 6 mol % of Mg had a lower value of mercury intrusion of 0.2522 mL/g than that determined for the MgHA1 pellet (2 mol % Mg, Fig. 5b). The low value is achieved by efficient packing of the precursor powder, which promoted by its fine particle size (average size 20 nm, Table 1), causing a reduction in the maximum pore size detected in this sample (0.5 μm) and HHP'ed pellets produced at different temperatures (0.06 μm , Fig. 5b). After conducting the HHP treatment at 150 $^{\circ}\text{C}$, the open porosity was reduced by up to 31.0 % and the reduction of porosity produced by the HHP at 240 $^{\circ}\text{C}$

was 35.0 %. The difference between the degree of porosity closure is associated with the particle packing of the green pellets, which depends on the nominal particle size of the precursor powder.

Moreover, the MgHA4 green pellet mercury intrusion cumulative curve showed a slight variation in comparison with the MgHA1 and MgHA3 green pellets (Fig. 5c). Few pores that were 10 μm in size were detected in this pellet, and the total mercury intrusion volume was 0.4549 mL/g. The curve exhibited two intrusion steps. The first step occurred over the pore range of 9.4 to 119 nm, while the second was visible over the pore size interval of 2.9 to 11 nm. These results indicated that a greater number of large pores was produced during the compaction of the green pellets prepared with micron particle sized MgHA4 powders in comparison to green pellets produced using powders with finer particle sizes (MgHA1 and MgHA3). When the MgHA4 powders underwent the HHP process, a reduction of the pore size was obtained. The maximum residual pore size was 200 nm. Likewise, the increase in the reaction temperature at 240 $^{\circ}\text{C}$ led to a remarkable reduction of the content of open porosity. In agreement with the mercury intrusion values measured, a decrease in porosity of 64.0 and 67.0 % was eliminated in pellets that were treated at 200 and 240 $^{\circ}\text{C}$, respectively. These results provide clear evidence that the remarkable reduction of porosity is likely enhanced by the reactivity of the MgHA powders with water under HHP conditions and this behaviour is irrespective of the initial MgHA particle size.

Based on the present results, we can argue that the chemical composition and particle size of the precursor powders are factors that enhance open porosity closure, which is likely achieved via particle packing initiated under HHP conditions. Hence, the evolution of the pore size distribution (PSD), which provides evidence of particle packing, was analysed against the increase in the treatment temperature and is shown in Fig. 6. For comparison purposes, the PSD of the green pellets was also included. In general, some differences in the PSD curves were observed by mercury intrusion analyses conducted at a high intrusion pressure (414 MPa) [36]. The MgHA3 (6 mol % Mg, mean particle size of 20 nm) green pellet showed a broad bimodal PSD with mean 16 and 33.1 nm pore sizes. The bimodal PSD prevailed on pellets subject to the HHP process at 150 and 200 $^{\circ}\text{C}$, but the pore size was further reduced as a result of the increase in the

particle packing at these temperatures. The further reaction between particles under HHP conditions above 200 °C promoted formation of a homogeneous residual PSD with a mean residual pore diameter of 11.3 nm (Fig. 6a). Likewise, a multimodal PSD curve was determined for the MgHA4 (1.5 µm particle size) green pellet, which had large pore size interval (3.1 and 316 nm). This distribution was broader than the distribution for the MgHA3 green pellet. The HHP consolidation of large particles produced a monomodal PSD with a mean pore diameter of 40 and 44.5 nm for pellets obtained at 200 and 240 °C, respectively. Homogenisation of the remaining PSD occurred faster than the homogenisation observed for the MgHA3 compacts, because the dissolution of the MgHA4 particles rapidly proceeded on the larger open porous network, allowing the recrystallisation of the new particles at nearly the same location. Thus, the HHP compaction process produces marked microstructural variations in the particulate phase and residual open porosity [25,29]. These results agree with the apparent density variation of the MgHA pellets (Fig. 4c) and therefore led us to conclude that HHP highly densified pellets have no close porosity.

Two different approaches were conducted to densify HA powders by the HHP technique. The first approach involved the in-situ formation of HA particles obtained by the chemical reaction between the precursor reactants and water [18-25]. The second approach consisted of the densification of chemically coprecipitated HA powders with water under hydrothermal hot pressing conditions. In both cases, the dissolution-precipitation mechanism is associated with the formation and densification of HA compacts [18,20], but the correlation between the particle size and chemical reactivity of the MgHA precursor with water has not yet been evaluated. This correlation may have a strong influence on enhancing the kinetics of the dissolution-recrystallisation mechanism associated with the packing process of the precursor MgHA powders, causing a remarkable densification at a relatively low temperature (200 °C). Based on the results mentioned above, we surmise that consolidation of MgHA powder by the HHP technology is enhanced by a one-step packing mechanism (Fig. 7), which is achieved as explained based on our results. Initially, the moistened MgHA precursor particles with small particle sizes loaded at 60 MPa, reached a relatively high apparent density (between 84.0 and 92.0 %, Table 2) due to the water surrounding their surfaces acting as a lubricant prior to the hydrothermal densification step. Subsequently, the adsorbed water rim reacted with the

MgHA particles after reaching the temperature of the HHP treatment. The packing mechanism involves localised dissolution of the MgHA particles [19] and simultaneous recrystallisation of smaller MgHA particles, which possibly occurs at the same location. This localised recrystallisation likely occurs gradually under intermediate and long reaction intervals due to hindered mass transfer induced by the constant pressure applied to the pellet (Fig. 7). In consequence, the gradual reduction in particle size improves the particle packing and limited crystal growth during the recrystallisation stage and also contributes to producing many new MgHA particles with fine sizes, and leads to a particle arrangement caused by constant loading, which closes the open porosity during the HHP process of the MgHA pellets. This inference is supported by our mercury intrusion results (Figs. 5 and 6). The proposed packing mechanism associated with the HHP technique that produced highly densified MgHA pellets is strongly affected by the densification reaction temperature and content of Mg in the MgHA structure.

3.4 Microstructural aspects and mechanical strength of MgHA compacts

Microstructural analyses of MgHA3 and MgHA4 conducted on the surface of green pellets and those of densified samples carried out after mechanical strength testing are included in Fig. 8. A large number of agglomerates (average size of 1.5 μm) of the MgHA3 particles were revealed in the green pellets, together with large porous with a mean size of 1.0 μm (Fig. 8a). However, the green pellet prepared with the MgHA4 particles (1.5 μm average size) show a remarkable amount of open porosity with different size varying in the range of 0.05 – 0.5 μm , as seen in Fig. 8d. Moreover, the densified compacts were obtained using 10 wt% water for 6 h at 200 and 240 $^{\circ}\text{C}$. In general, the FE-SEM micrographs show that a particle size reduction occurred after compression. In particular, for the MgHA4 compact subjected to the HHP treatment at 200 $^{\circ}\text{C}$ (Fig. 8e), which consisted of elongated particles of approximately 0.4 μm in size and a reduced number of small rod-shaped particles with an average size of 0.075 μm . A similar packing behaviour was observed for the MgHA3 pellets, although particles agglomerates with a mean size of 0.1 μm were also observed (Figs. 8b and 8c). The compacted pellets MgHA3 and MgHA4 produced at 240 $^{\circ}\text{C}$ exhibited a well-packed

microstructure composed of very fine particles with average sizes of 0.05 and 0.08 μm , respectively; in comparison with their original particle size in the green pellet, and therefore the porosity was not visible in the FE-SEM micrographs (Fig 8c and 8f). The marked reduction in particle size that resulted from the packing process occurred regardless of the Mg content of the precursors and took place as a consequence of the dissolution-recrystallisation mechanism. The microstructural features observed on both green and HHP'ed pellets are in good agreement with the porosity distribution results (Figs. 5 and 6), and overall, they support the packing mechanism proposed for producing MgHA highly densified pellets at low temperatures (< 240 $^{\circ}\text{C}$) by the HHP process.

The variation of the mechanical strength, as determined by diametral compression, is only discussed as a function of the reaction temperature because this was the relevant parameter that produced highly densified MgHA pellets. The results of the tensile strength of MgHA1, MgHA3 and MgHA4 pellets prepared in this study are shown in Fig. 9. The error bars included for each average value provide statistical analysis, indicating the systematic variation of the mechanical strength for the three MgHA specimens compacted, and all of the values are within error propagation and no overlapping of the tensile strength values is visible in Fig. 9. This phenomenon indicates the confidence in the mechanical measurement conducted for the MgHA pellets subjected to the HHP process in the present work. Although, the tensile strength results might be analogous to the apparent density results (Fig. 4c), it can be argued that the tensile strength depends on the packing process that occurs during the HHP process. The highly compacted MgHA3 pellets exhibited the highest values of tensile strength (12.2 ± 0.6 MPa) and a slight linear increase in the mechanical strength occurred increasing the reaction temperature. By contrast, a notorious increase in the strength was observed to occur above 200 $^{\circ}\text{C}$ for the samples MgHA1 and MgHA4 (Fig. 9). The maximum values of tensile strength achieved for these samples were 10.6 ± 0.9 MPa and 3.7 ± 1.7 MPa, respectively. Moreover, a marked threefold difference of the strength between the MgHA3 (12.6 ± 0.6 MPa) and MgHA4 pellets containing 6 mol % Mg was observed, even though the MgHA4 pellets reached high apparent densities (3.0471 g/cm^3). The decrease of the strength of the MgHA pellets is likely attributed to the incipient particle bonding produced during the microstructural rearrangement of the recrystallised fine new particles. The maximum

tensile strength values for the MgHA3 precursors (6 mol % Mg, nominal average size of 20 nm) are consistent with those reported for the densification of HA pellets under HHP conditions reported in the literature [25,27]. Based on these results, we suggest that the tensile strength attained for MgHA powders resulted from the cohesion and packing of particles during the dissolution-recrystallisation mechanism under HHP densification conditions. Particles with a nanometre-order size rapidly achieved a homogeneous arrangement of the new recrystallised particles with a reduction in porosity, which improved the tensile strength of the MgHA powders.

The present densification technique coupled with a post-high temperature sintering stage might be used to rapidly prepare monolithic MgHA bioceramics, because the high apparent relative density and low porosity content are likely to reduce the atomic diffusion distance between MgHA particles in the pellets, even at relative mild sintering temperatures (800–900 °C). The present hypothesis is experimentally supported by the results reported at the beginning of the current decade by one of the present authors [22]. Who firstly proposed the processing technology for accelerating the solid-state sintering stage of calcium hydroxyapatite powders, which involves a preliminary particle consolidation step conducted under constant loading and assisted by a hydrothermal reaction at very low temperatures (150 – 200 °C). Typically, the compacts with a bulk density of 61.0 % obtained at standard HHP conditions at 200 °C with a loading pressure of 60 MPa for 2 h and 10 wt% water content. The specimens were rapidly sintered to bulk density values of up to 95.0 % at temperatures over 1200 °C for the short time of 2 h [22]. The coalescence of pores that produce the close porosity coupled with the grain growth slightly decelerates the increase of both the bulk and apparent density over the temperature range of 800 – 1000 °C. In general, the vast research work conducted last two decades on the HAp low-temperature powder densification. It has been based on the hydrothermal reaction kinetics principals and mechanisms [37-39], which were determined for various inorganic [40-44] and organic [45] powders at temperatures in the range of 100 – 300 °C that reacted with water and alkaline medium under HHP conditions. Likewise, a new technology for sintering ceramic materials named as hydrothermal-assisted cold sintering process has recently been proposed, which involves hydrothermal reaction fundamentals in a broad variety of aqueous solutions [46]. Also, this technique has been extended to the study of the hydrothermal

sintering of various inorganic materials that dissolves congruently in an alkaline medium including BaTiO₃, among others [46]. Hence, the present study of densification for MgHA compacts prepared under HHP conditions is being undertaken to determine their sintering behaviour at high temperatures, to prepare MgHA monolithic bioceramics with a controlled microstructure and strength similar to that of cortical bone.

4. Conclusions

Densification of MgHA precursor powders was successfully achieved to high apparent density values varying between 2.9124 – 3.0758 g/cm³ at low temperature under hydrothermal hot pressing conditions. Compacted pellets were prepared using microwave-hydrothermally synthesised fine MgHA powders with three different Mg contents (2, 4 and 6 mol % Mg). The HHP technique promoted remarkable particle densification without thermal dehydration or decomposition of the small particle size powders. This process involved the chemical reaction between MgHA particles and 10 wt% water at reasonably low temperatures (150 °C) under hydrothermal conditions. The reaction was maintained for 6 h at a constant loading pressure of 60 MPa. The one-step mechanism of densification at low temperature involves continuous dissolution-recrystallisation of the bulk particles that depends on the Mg content of the MgHA precursor powders and temperature rather than on the particle size. Therefore, a higher content of Mg (6 mol %) in the HA structure and a high reaction temperature (240 °C) enhance the densification of the hydrothermal microwave producing MgHA powders. The low-temperature HHP technique allows a systematic microstructural rearrangement of particles, favouring the formation of pellets with high relative apparent densities (> 95.0 %), even with a large particle size (1.5 µm). The MgHA3 pellet, which had a maximum relative apparent density of 98.2 % had a high tensile strength of 12.6 ± 0.5 MPa, which was achieved using standard experimental conditions (240 °C, 6 h, 10 wt% water) as result of high particle packing and partial particle cohesion. However, low particle cohesion was markedly produced in pellets subjected to the HHP process prepared with the large sized MgHA4 powder, which reached a maximum tensile strength of only 3.7 ± 1.7 MPa at 240 °C for 6 h (apparent density of 3.0425 g/cm³). The present low-temperature densification process in combination with high temperature sintering is likely an alternative route for processing monolithic dense MgHA bioceramics for

biomedical applications.

Acknowledgments

The authors acknowledge CONACYT - México for supporting the present research work through the research grant CB-2008-01-0107052. J.C.R.A and Z.M.V are indebted to CONACYT-SNI. K.L.M.C. is indebted to the National Council for Science and Technology of Mexico, for its financial support as a Ph.D. scholarship. Many thanks are also given to Professor T. Yamamoto and Dr. T. Matsuzaki from the Centre for Advanced Marine Core Research, Kochi University, Japan, for their assistance with FE-scanning electron microscopy. Dr. T. Kono at Kochi Prefectural Industrial Technology Centre, Kochi Japan, is gratefully acknowledged for his valuable assistance in conducting the mechanical characterisation of compacted specimens.

5. References

- [1] R. Z. LeGeros. Calcium phosphates in oral biology and medicine, in H. M. Myers (Ed.), *Monogr Oral Sci.* Basel, Karger., New York, 1991, pp 4-45.
- [2] H. Zhou, J. Lee, Nanoscale hydroxyapatite particles for bone tissue engineering. *Acta Biomater.* 7 (2011) 2769–2781.
- [3] E. Boanini, M. Gazzano, A. Bigi. Ionic substitutions in calcium phosphates synthesized at low temperatura. *Acta Biomater.* 6 (2010) 1882–1894.
- [4] S. Kannan, F. Goetz-Neunhoeffler, J. Neubauer, and J. M. F. Ferreira. Ionic Substitutions in Biphasic Hydroxyapatite and β -Tricalcium Phosphate Mixtures: Structural Analysis by Rietveld Refinement. *J. Am. Ceram. Soc.* 91 (2008) 1–12.

- [5] M. P. Staiger, A. M. Pietak, J. Huadmai, G. Dias. Magnesium and its alloys as orthopedic biomaterials: A review. *Biomaterials* 27 (2006) 1728–1734.
- [6] T. Okuma. Magnesium and Bone Strength. *Nutrition*. 17 (2001) 679–680.
- [7] W. Mroz, A. Bomblaska, S. Burdynska, M. Jedynski, A. Prokopiuk, B. Budner, A. Slosarczyk, A. Zima, E. Menaszek, A. Scislowska-Czarnecka, K. Niedzielski. Structural studies of magnesium doped hydroxyapatite coatings after osteoblast culture. *J. Mol. Struct.* 977 (2010) 145–152.
- [8] N-E.L. Saris, E. Mervaala, H. Karppanen, J.A. Khawaja, A. Lewenstam. Review Magnesium An update on physiological, clinical and analytical aspects. *Clin. Chim. Acta* 294 (2000) 1–26.
- [9] J. Vormann. Magnesium: nutrition and metabolism. *Mol. Asp. Med.* 24 (2003) 27–37.
- [10] E. Landi, A. Tampieri, M. Mattioli-Belmonte, G. Celotti, M. Sandri, A. Gigante, P. Fava, G. Biagini. Biomimetic Mg- and MgCO_3 substituted hydroxyapatites: synthesis characterization and in vitro behaviour. *J. Eur. Ceram. Soc.* 26 (2006) 2593–2601.
- [11] W.L. Suchanek, K. Byrappa, P. Shuk, R.E. Riman, V.F. Janas, K.S. TenHuisen. Preparation of magnesium-substituted hydroxyapatite powders by the mechanochemical–hydrothermal method. *Biomaterials*. 25 (2004) 4667–4657.
- [12] E. Landi, A. Tampieri, G. Celott, M. Mattioli Belmonte, G. Logroscino. Synthetic Biomimetic Nanostructured Hydroxyapatite. *Key Eng. Mater.* ISSN:1662-9795. Vols. 284-286, 949–952.
- [13] E. Landi, G. Logroscinno, L. Proietti, A. Tampieri, M. Sandri, S. Sprio. Biomimetic Mg-substituted hydroxyapatite: from synthesis to in vivo behaviour. *J Mater Sci: Mater. Med.* 19 (2008) 239–247.
- [14] L. Stipniece, K. Salma-Ancanea, N. Borodajenko, M. Sokolova, D. Jakovlevs, L. Berzina-Cimdina. Characterization of Mg-substituted hydroxyapatite synthesized by wet chemical method. *Ceram. Int.* 40 (2014) 3261–3267.

- [15] I. Cacciotti, A. Bianco, M. Lombardi and L. Montanaro; Mg-substituted hydroxyapatite nanopowders: Synthesis, thermal stability and sintering behaviour. *J. Eur. Ceram. Soc.* 29 (2009) 2969–2978.
- [16] J.R. Groza and R.J. Jhwding. Nanoparticulate Materials Densification. *NanoStructured Mater.* 7 (1996) 749–768.
- [17] R.L. Pober, E.A. Barringer, M.V. Parish, N. Levoy and H.K. Bowen. Dispersion and packing of narrow size distribution ceramic powders. In *Emergent Process Methods for High-Technology Ceramics. Series Materials Science Research.* Springer US, 1984, 193–206.
- [18] A. Nakahira and T. Murakami. Fabrication of Porous Hydroxyapatite Using Hydrothermal Hot Pressing and Post-Sintering. *J. Am. Ceram. Soc.* 88 (2005) 1334–1336.
- [19] J. Li, T. Hashida. Preparation of hydroxyapatite ceramics by hydrothermal hot-pressing method at 300 °C. *J. Mater. Sci.* 42 (2007) 5013–5019.
- [20] K. Yanagisawa, J.H. Kim, C. Sakata, A. Onda, E. Sasabe, T. Yamamoto, Z. Matamoros-Veloza, J.C. Rendón-Angeles. Hydrothermal Sintering under Mild Temperature Conditions: Preparation of Calcium-deficient Hydroxyapatite Compacts. *Z. Naturforsch.* 65 (2010) 1038–1044.
- [21] J.G. Li and T. Hashida. In situ Formation of Hydroxyapatite-Whisker Ceramics by Hydrothermal Hot-Pressing Method. *J. Am. Ceram. Soc.* 89 (2006) 3544–3546.
- [22] J.H. Kim, K. Yanagisawa, A. Onda, E. Sasabe, T. Yamamoto. Densification behavior of hydroxyapatite green pellets prepared by different methods. *J. Am. Ceram. Soc. Jpn.* 123 (2015) 1097–1101.
- [23] N. Yamasaki, T. Kai, M. Nishioka, K. Yanagisawa, K. Ioku. Porous hydroxyapatite ceramics prepared by hydrothermal hot-pressing. *J. Mater. Sci. Lett.* 9 (1990) 1150–115.
- [24] K. Ioku, K. Yamamoto, K. Yanagisawa. Low temperature sintering of hydroxyapatite by hydrothermal

- hot-pressing. Phosphorus Res. Bull. 4 (1994) 65–70.
- [25] K. Yanagisawa, T. Fujino, K. Zhu, K. Ioku, A. Onda, K. Kajiyoshi, C.W. Chen and R.E. Riman. Development of low temperature sintering of hydroxyapatite ceramics using hydrothermal hot-pressing method. Phosphorus Res. Bull. 17 (2004) 231–234.
- [26] S. Ishihara, T. Matsumoto, T. Onoki, T. Sohmura, A. Nakahira. New concept bioceramics composed of octacalcium phosphate (OCP) and dicarboxylic acid-intercalated OCP via hydrothermal hot-pressing. Mater. Sci. Eng. C 29 (2009) 1885–1888.
- [27] K. Hosoi, T. Hashida, H. Takahashi, N. Yamasaki, and T. Korenaga. New Processing Technique for Hydroxyapatite Ceramic by the Hydrothermal Hot-Pressing Method. J. Am. Ceram. Soc. 79 (1996) 2771–2774.
- [28] Y. Mizutani, M. Hattori, M. Okuyama, T. Kasuga, M. Nogami. Large-sized hydroxyapatite whiskers derived from calcium tripolyphosphate gel. J. Eur. Ceram. Soc. 25 (2005) 3181–3185.
- [29] N. Yamasaki, K. Yanagisawa, M. Nishioka, S. Kanahara. A hydrothermal hot-pressing method: apparatus and application. J. Mater. Sci. Lett. 5 (1986) 355–356.
- [30] M. Mellor, Ivor Hawkes. Measurement of Tensile Strength by Diametrical Compression of Discs and Annuli. Eng. Geol. 5 (1971) 173–225.
- [31] International Society for Rock Mechanics Commission on Standardization of Laboratory and Field Tests, “Suggested methods for Determining Tensile Strength of Rock Materials,” Int. J. Rock. Mech. Min. Sci. Geomech. Abstr. 15 (1978) 99–103.
- [32] ASTM Standard C128-15, Standard Test Method for Relative Density (Specific Gravity) and Absorption of Fine Aggregate¹, ASTM International, West Conshohocken, PA 19428-2959. DOI:10.1520/C0128-15.

- [33] A.A. Chaudhry, J. Goodall, M. Vickers, J.K. Cockcroft, I. Rehman, J.C. Knowles, J.A. Darr. Synthesis and characterisation of magnesium substituted calcium phosphate bioceramic nanoparticles made via continuous hydrothermal flow synthesis, *J. Mat. Chem.* 18 (2008) 5900-5908.
- [34] P. Feng, M. Niu, C. Gao, S. Peng, C. Shuai. A novel two-step sintering for nano-hydroxyapatite scaffolds for bone tissue engineering. *Sci. Rep.* 4:5599 (2014) 1–10.
- [35] H. Giesche. Mercury Porosimetry: A General (Practical) Overview. *Part. Part. Syst. Charact.* 23 (2006) 1-11.
- [36] Ernesto Borrelli, “ARC Laboratory Handbook: Porosity”, International Centre for the Study of the Preservation and Restoration of Cultural Property (ICCROM 1999), ISBN 92-9077-157-7.
- [37] B. Scott and T. G. Carruthers. Hydrothermal reactions and crystallographic relationships found during the reactive hot pressing of kaolinites. *Clay Minerals* 8 (1969) 21-28.
- [38] N. Yamasaki, K. Yanagisawa, M. Nishioka, S. Kanahara. A hydrothermal hot-pressing method: Apparatus and application. *J. Mater. Sci. Lett.* 5 (1986) 355-356.
- [39] K. Yanagisawa, M. Nishioka, N. Yamasaki. Neck formation of spherical silica particles by hydrothermal hot pressing. *J. Mater. Sci. Lett.* 10 (1991) 7-8.
- [40] K. Yanagisawa, M. Nishioka, N. Yamasaki. Solidification of powders in $\text{SiO}_2\text{-Fe}_2\text{O}_3$ and $\text{SiO}_2\text{-ZrO}_2$ system by hydrothermal hot pressing, *Yogyo Kyokai-Shi*, 94 (1986) 1193-1196.
- [41] M. Nishioka, S. Hirai, K. Yanagisawa, N. Yamasaki. Solidification of glass powder with simulated high-level radioactive waste during hydrothermal hot-pressing. *J. Am. Ceram. Soc.* 73 (1990) 317-322.
- [42] N. Yamasaki, Tang Weiping, Ke Jiajun, K Hosoi. Low-temperature sintering of calcium and magnesium carbonate by the hydrothermal hot-pressing technique. *J. Mater. Sci. Lett.* 14 (1995) 1268-1270.

- [43] K. Sato, T. Hashida, H. Takahashi, N. Yamasaki. Development of high strength calcium aluminate-phosphate cement by hydrothermal hot-pressing. *J. Mater. Sci. Lett.* 16 (1997) 1464–1468.
- [44] K. Hosoi, T. Hashida, H. Takahashi, N. Yamasaki, T. Korenaga. Solidification behaviour of calcium carbonate via aragonite–calcite wet transformation with hydrothermal hot pressing. *J. Mater. Sci. Lett.* 16 (1997) 382–385.
- [45] M. Kaneko. Solidification of ion-exchange resins by hydrothermal hot-pressing. *J. Mater. Sci. Lett.* 12 (1993) 591-593.
- [46] H. Guo, J. Guo, A. Baker, C.A. Randall. Hydrothermal-assisted cold sintering process: A new guidance for low-temperature ceramic sintering. *Appl. Mater. Interfaces*, 8 (2016) 20909-20915.

Fig. 1. (a) XRD patterns of raw MgHA powders prepared under microwave-hydrothermal conditions at 150 °C for 1 h. TEM micrographs of (b) MgHA1, (c) MgHA3 and (d) MgHA4 (d) precursor powders.

Fig. 2. XRD patterns of MgHA pellets compacted under HHP conditions at 200 °C for 6 h with a mixing water content of 10 wt%.

Fig. 3. FT-IR spectra of MgHA3 pellets after the densification for 6 h with a mixing water content of 10 wt% at different temperatures.

Fig. 4. Variation of the apparent density of MgHA green pellets and pellets prepared under HHP conditions: (a) at 200 °C for 6 h with different water contents, (b) at 200 °C with 10 wt% for various reaction times and (c) with 10 wt% of water for 6 h at different temperatures. (nominal particle size: ▲ 39 nm MgHA1, ■ 32

nm MgHA2, ● 20 nm MgHAp and ◆ 1.5 μm MgHA4).

Fig. 5. Variation of cumulative mercury intrusion with the pore size of the green pellets and MgHA pellets prepared under HHP conditions with 10 wt% of water for 6 h at different temperatures for (a) MgHA1, (b) MgHA3, and (c) MgHA4 precursor powders.

Fig. 6. Differences of the pore size distribution of green pellets and (a) MgHA3, and (b) MgHA4 disks subjected to the HHP process prepared at a constant loading pressure of 60 MPa for 6 h with a water content of 10 wt% at different temperatures.

Fig. 7. Schematic representation of the densification mechanism for the low temperature HHP technique involving a dissolution-recrystallisation step that promotes densification of the MgHA powder precursor and homogenisation of the residual porosity.

Fig. 8. SEM micrographs of the fracture surface of the (a) MgHA3 and (d) MgHA4 green pellets. Also, those of the samples densified under HHP conditions at a loading pressure of 60 MPa using 10 wt% water at 200 °C: (b) MgHA3, (e) MgHA4, and 240 °C (c) MgHA3, (f) MgHA4.

Fig. 9. Variation of the tensile strength for MgHA pellets obtained under HHP conditions with 10 wt% of water for 6 h at different temperatures.

Table 1 Physical characteristic of starting MgHA powders with different Mg concentration produced by hydrothermal microwave-assisted treatments at 150 °C for 1 h using two different phosphate compounds.

Chemical and physical characteristics	Sample ID			
	MgHA1	MgHA2	MgHA3	MgHA4
Phosphorus precursor reagent		$(\text{NH}_4)_2\text{HPO}_4$		$\text{Na}_5\text{P}_3\text{O}_{10}$
Mg nominal composition (mol %)	2	4	6	6
Chemical formula ^a	$\text{Ca}_{9.80}\text{Mg}_{0.20}(\text{PO}_4)_6(\text{OH})_2$	$\text{Ca}_{9.59}\text{Mg}_{0.41}(\text{PO}_4)_6(\text{OH})_2$	$\text{Ca}_{9.39}\text{Mg}_{0.61}(\text{PO}_4)_6(\text{OH})_2$	$\text{Ca}_{9.41}\text{Mg}_{0.59}(\text{PO}_4)_6(\text{OH})_2$
Crystallite size (nm) ^b	39	32	20	1505.58
Ultimate density (g/cm^3) ^c	3.1389	3.1384	3.1298	3.1321
Crystallite size (nm) ^d	63.8	62.71	62.26	1400
Superficial area (m^2/g) ^e	63.58	70.43	83.27	20.28

^a The chemical formula of the MgHA was calculated from the contents of Ca, Mg and P determined via ICP-AES and OH^- was calculated by charge balance.

^bCrystallite size measured by Rietveld refinement.

^cUltimate density calculated using the lattice constant of the unit cell, chemical formula weight and Avogadro number.

^dCrystallite size measured from the TEM micrographs.

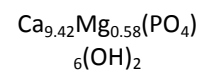
^eThe superficial area was determined using BET N₂ adsorption isotherms analysis.

Table 2. Summary of the HHP treatments of MgHA fine powders.

Sample ID (MgHA p#)	Precursor average particle size	Mg ²⁺ Composition (mol %)	Temperature (°C)	Time (h)	Water content (wt%)	Apparent Density (g/cm ³)		Open porosity (%) ^c	Chemical composition of MgHAp pellets ^d
						[%] ^a	(g/cm ³) ^b		
MgHA1-1*	39 nm	2	-	0.08	-	-	2.9135 ± 0.009 [92.82]	7.18	Ca _{9.81} Mg _{0.19} (PO ₄) ₆ (OH) ₂

MgHA1- 2	2	150	6	10	3.0501[96 .89]	2.912 4 ± 0.028 [93.00]	6.96
MgHA1 -3	2	200	6	10	3.0689[97 .49]	2.956 4 ± 0.036 [94.10]	4.66
MgHA1- 4	2	240	6	10	3.0727[98 .45]	2.965 1 ± 0.042 [94.46]	4.19
MgHA3- 1*	6	-	0.0 8	-	-	2.953 7 ± 0.032 [94.37]	5.62
MgHA3- 2	6	150	6	10	3.0943[98 .58]	3.003 9 ± 0.009 [95.97]	3.71
MgHA3- 3	6	200	6	10	3.1120[99 .14]	3.062 2 ± 0.024 [97.84]	2.93
MgHA3- 4	6	240	6	10	3.1234[99 .50]	3.075 8 ± 0.001 [98.28]	1.73

20 nm



MgHA3-5	6	200	1	10	3.0566[97 .37]	3.000 9 ± 0.004 [95.88]	4.27
MgHA3-6	6	200	2	10	3.0730[97 .90]	3.021 7 ± 0.027 [96.54]	4.34
MgHA3-7	6	200	4	10	3.0897[98 .43]	3.041 1 ± 0.018 [97.16]	3.43
MgHA3-8	6	200	6	15	3.1203[99 .40]	3.055 5 ± 0.014 [97.62]	1.76
MgHA3-9	6	200	6	20	3.1245[99 .54]	3.059 9 ± 0.009 [97.76]	1.93
MgHA4-1*	6	-	0.0 8	-	-	2.608 7 ± 0.092 [83.29]	16.71
MgHA4-2	6	150	6	10		2.963 7 ± 0.035 [94.62]	4.24

1.5 μm

$\text{Ca}_{9.42}\text{Mg}_{0.58}(\text{PO}_4)_6(\text{OH})_2$

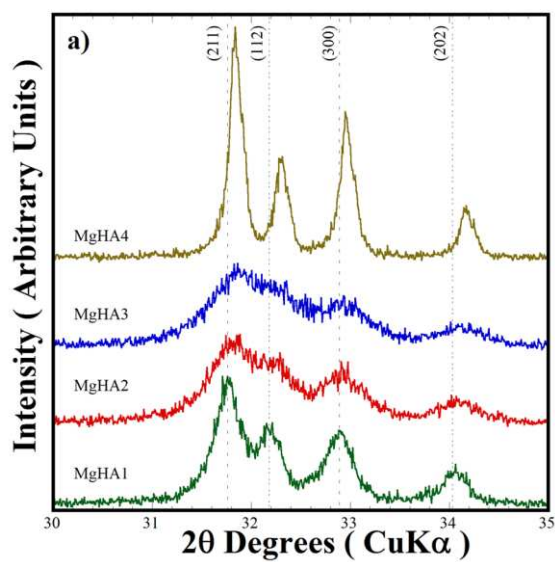
MgHA4-3	6	200	6	10	2.9978[96 .05]	2.984 4 ± 0.018 [95.28]	4.11
MgHA4-4	6	240	6	10	3.0858[98 .02]	3.042 5 ± 0.024 [97.13]	2.71
MgHA4-5	6	200	1	10	2.8778[92 .21]	2.939 4 ± 0.045 [93.84]	4.71
MgHA4-6	6	200	2	10	2.9397[94 .19]	2.958 7 ± 0.043 [94.46]	4.14
MgHA4-7	6	200	4	10	2.9506[95 .54]	2.964 6 ± 0.037 [94.61]	4.14
MgHA4-8	6	200	6	15	3.0008[96 .15]	3.010 1 ± 0.010 [96.10]	3.16
MgHA4-9	6	200	6	20	3.0028[96 .21]	3.014 0 ± 0.022 [96.22]	3.04

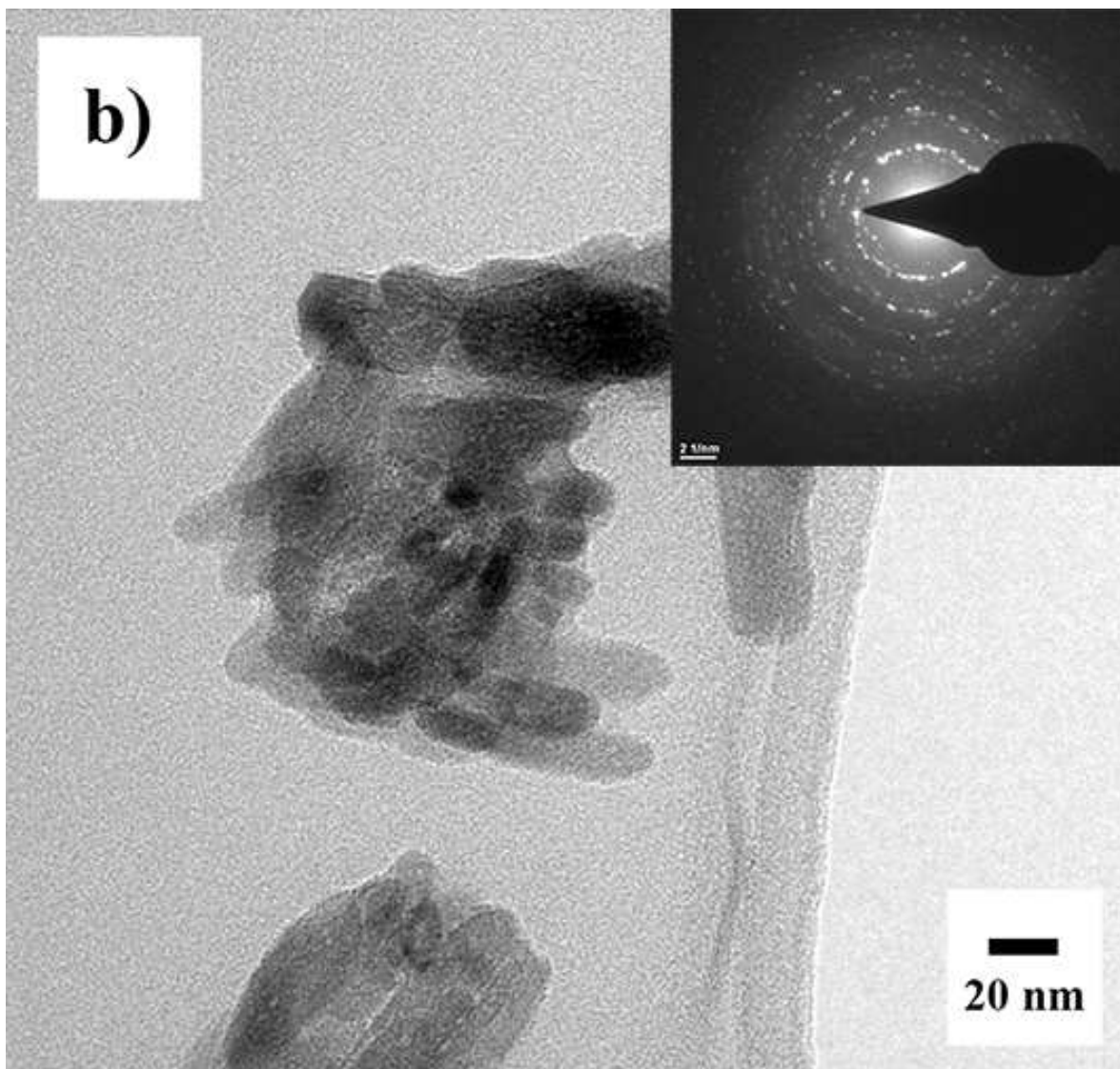
^a Apparent density determined by means of the Archimedes' method using boiling water.

^b Apparent density determined by He-pycnometry.

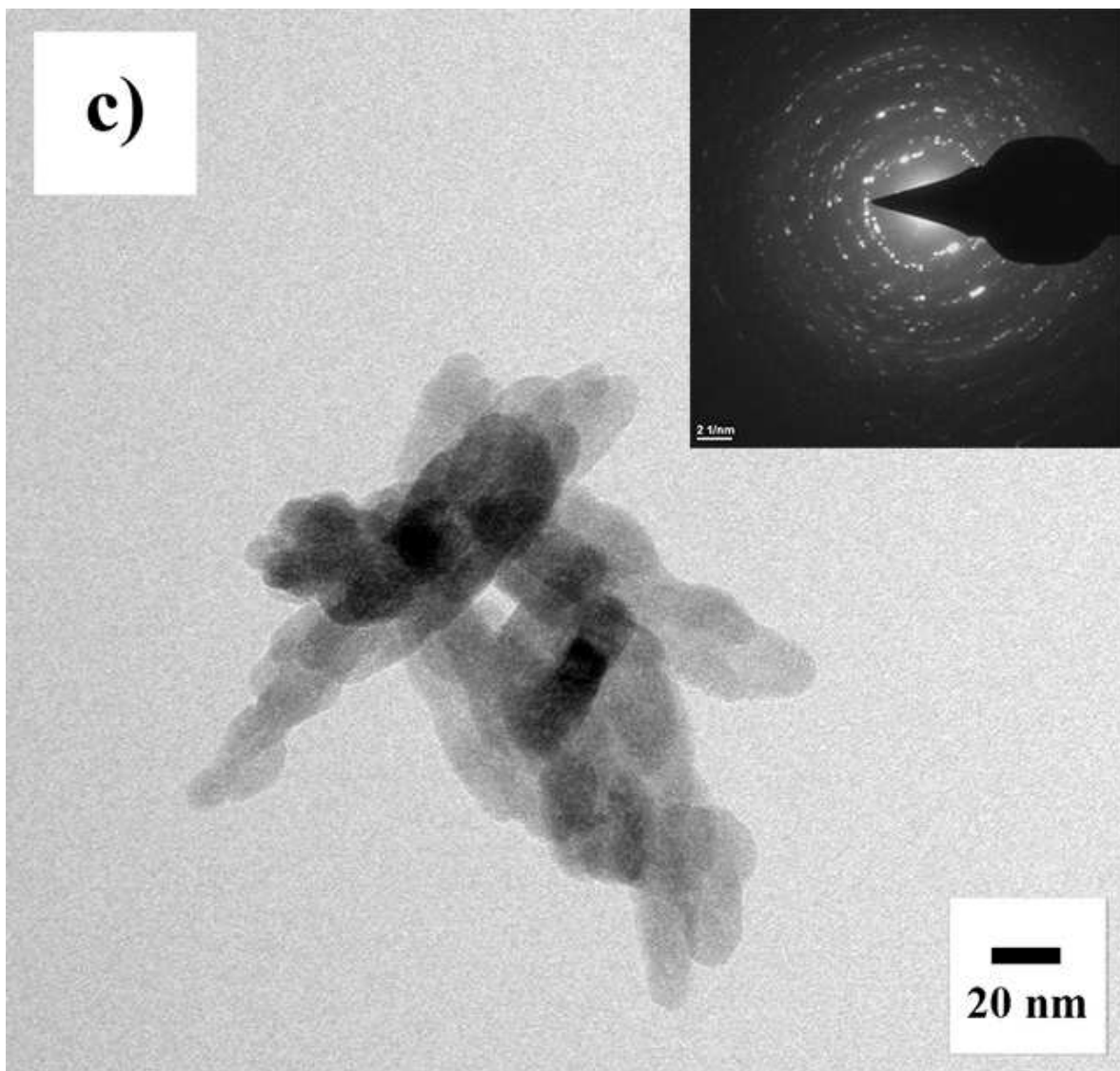
^c Open porosity computed from values of ultimate density and apparent density measured by Helium-pycnometer.

^d The chemical formula of the sample powders was calculated from the contents of Ca, Mg and P determined via ICP-AES and OH⁻ was calculated by charge balance.

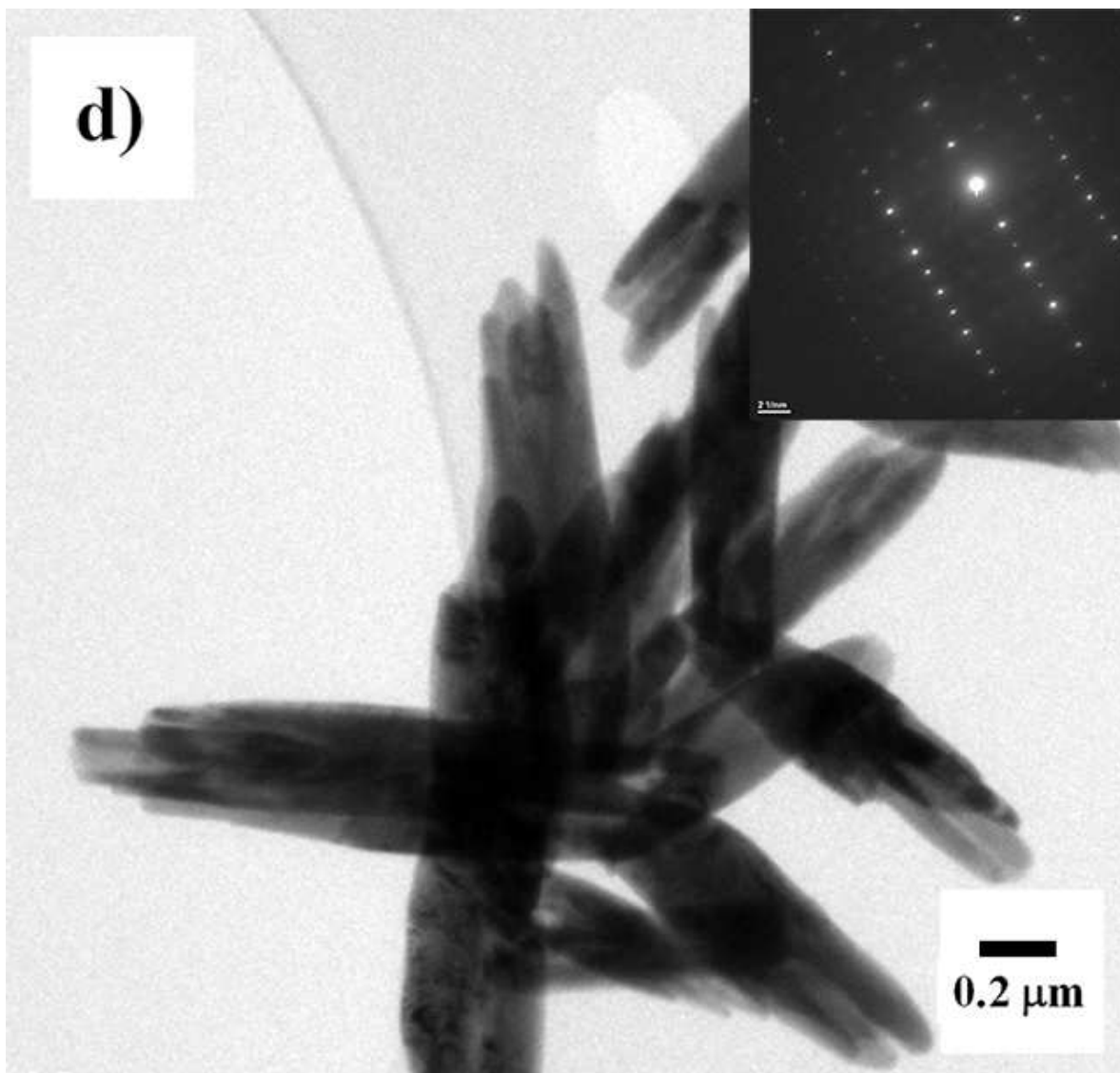




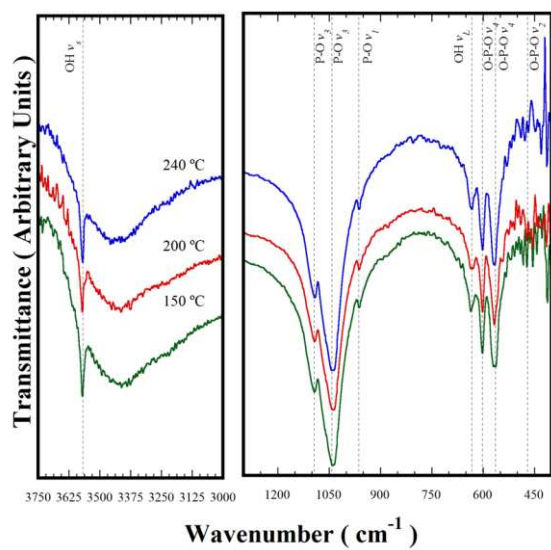
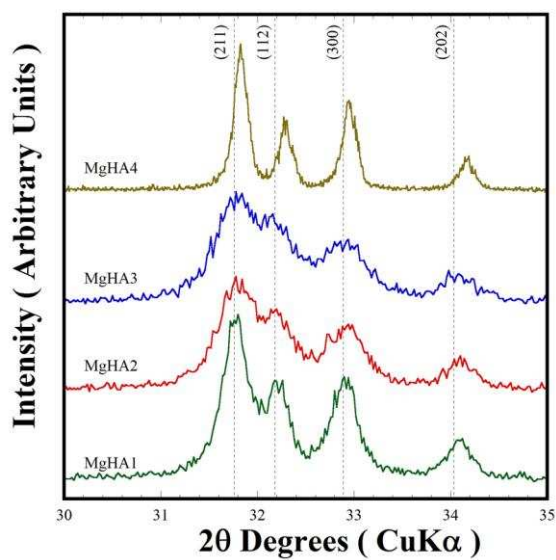
ACCEPTED

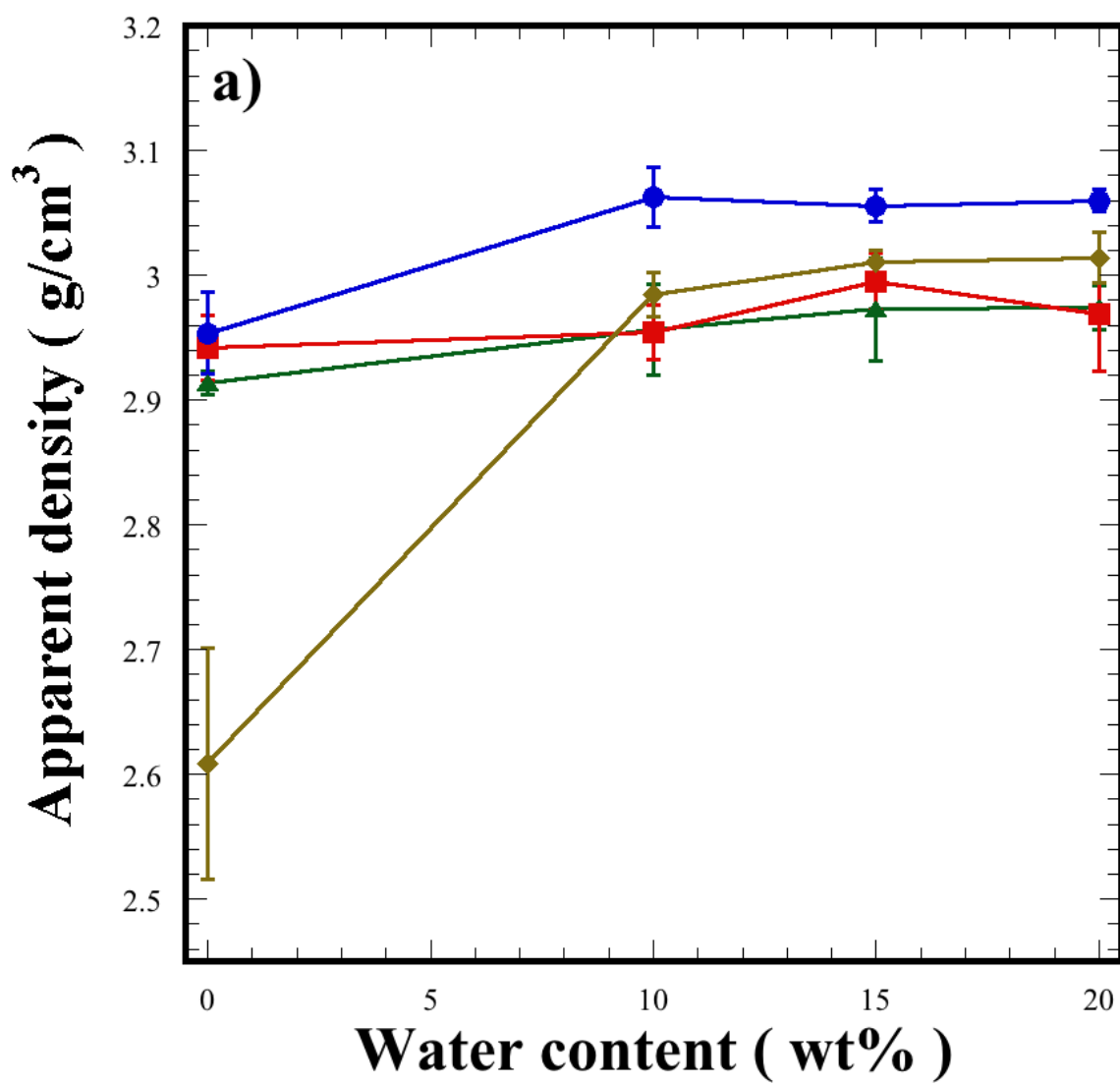


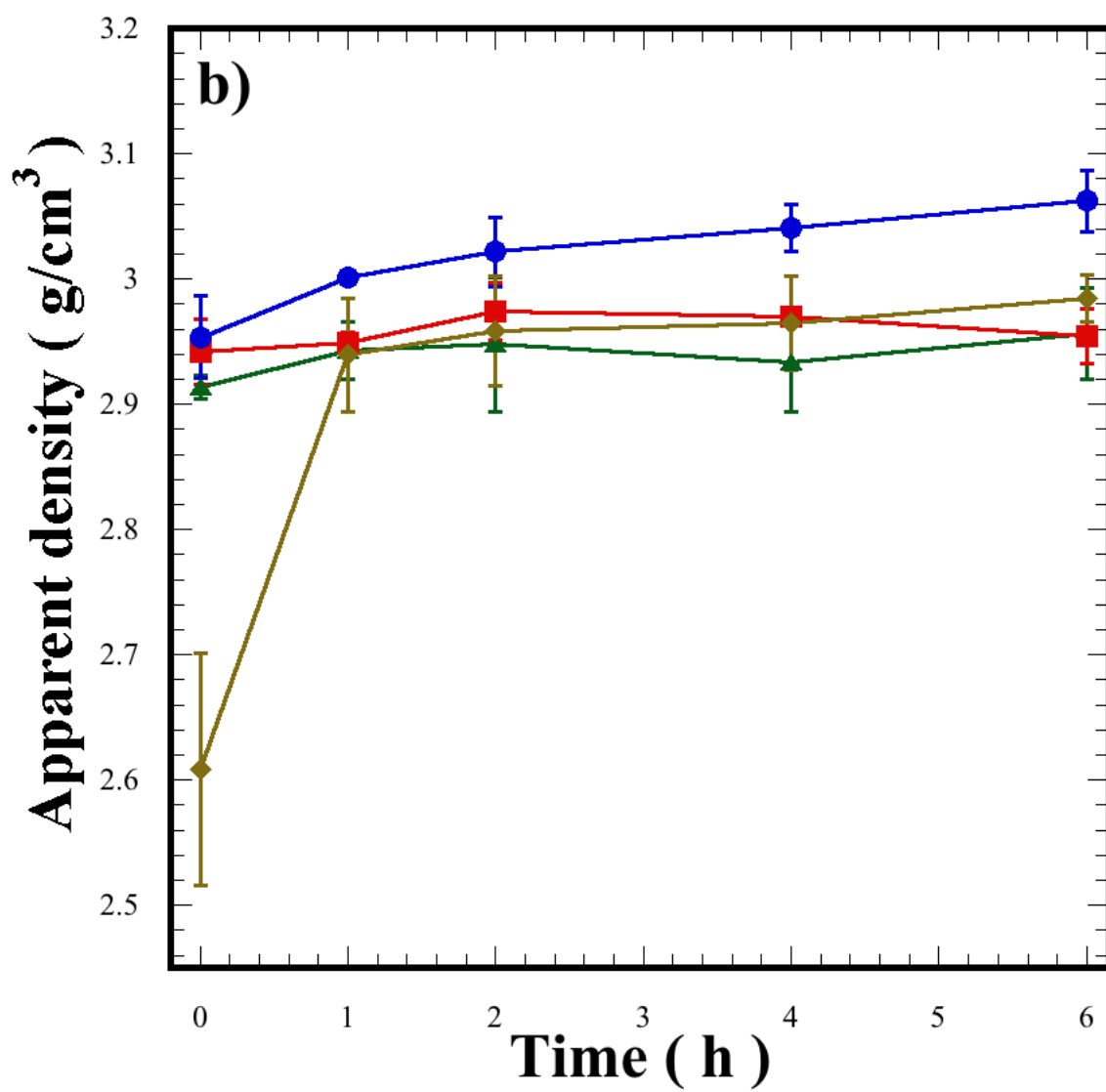
Acc



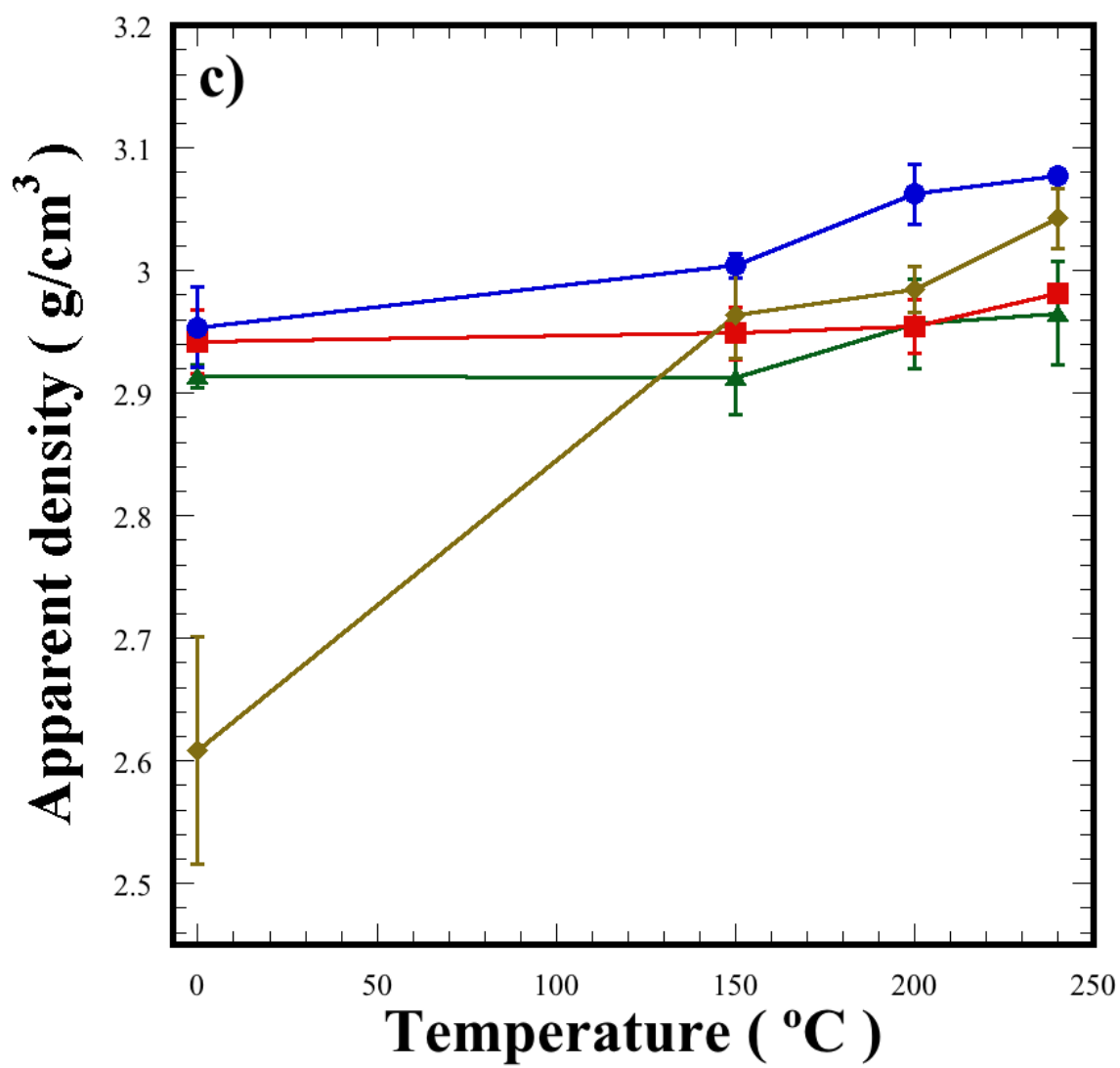
ACC

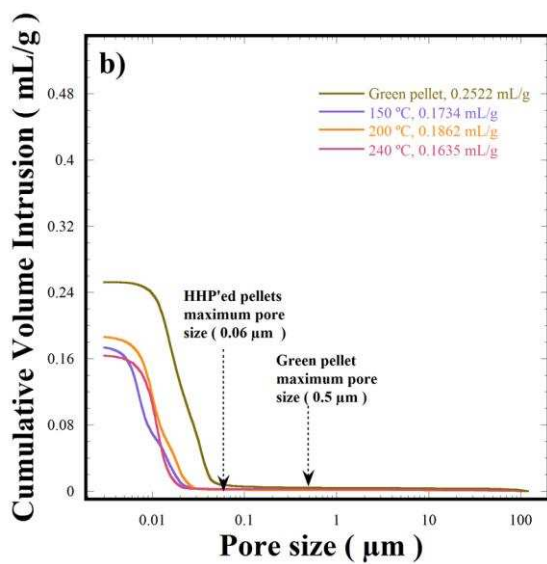
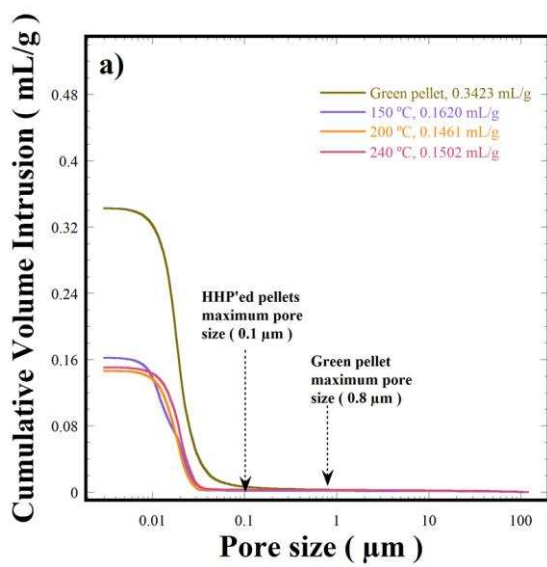


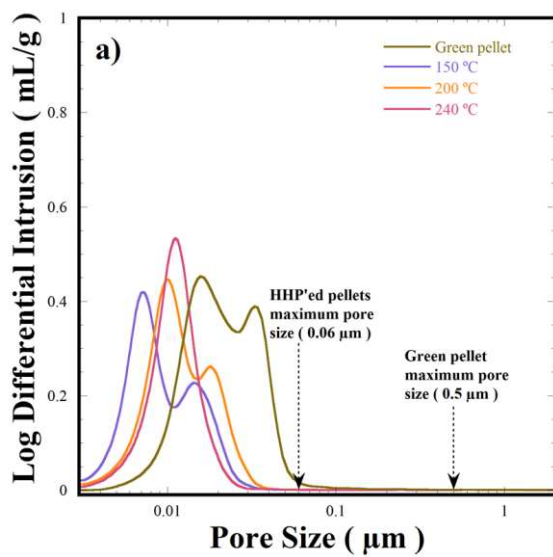
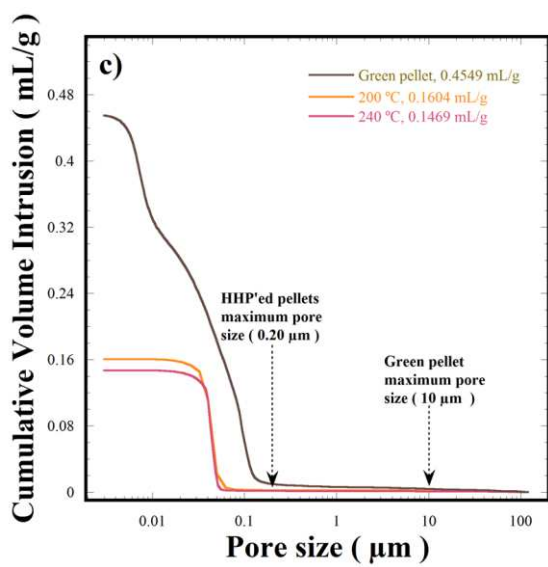


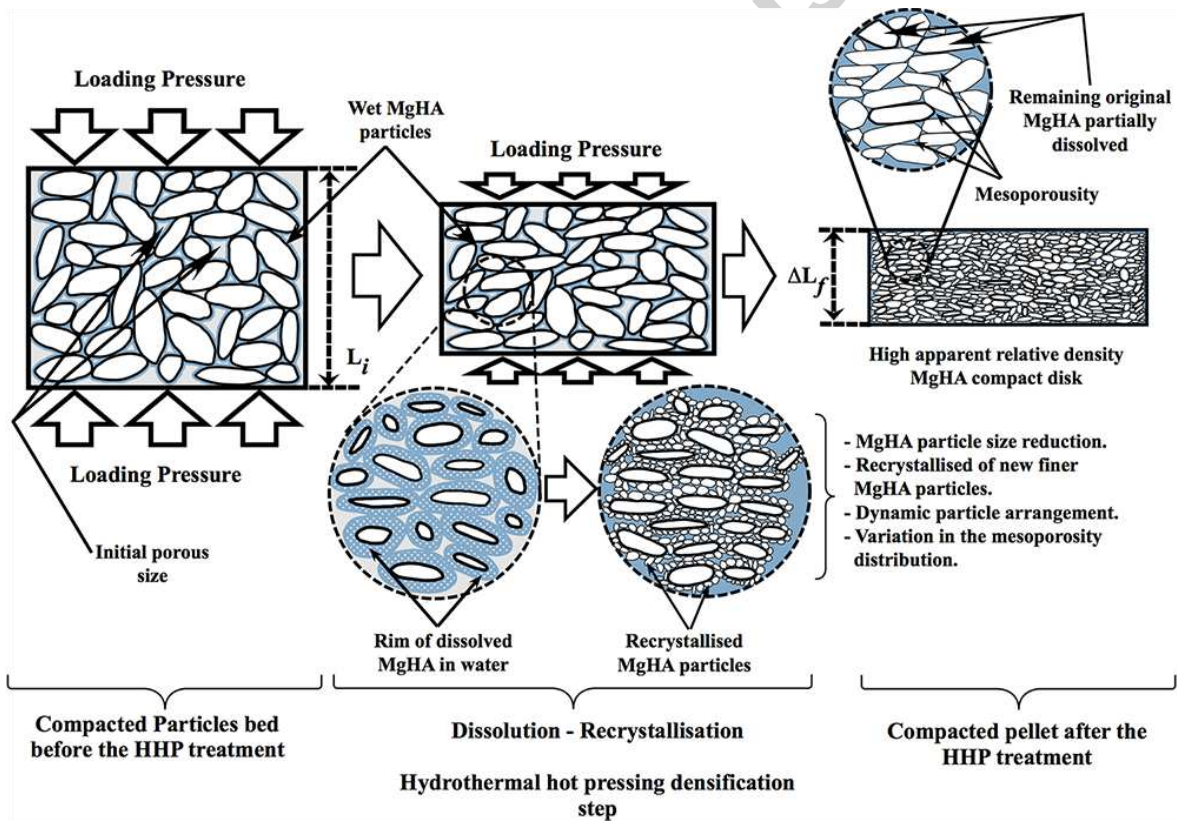
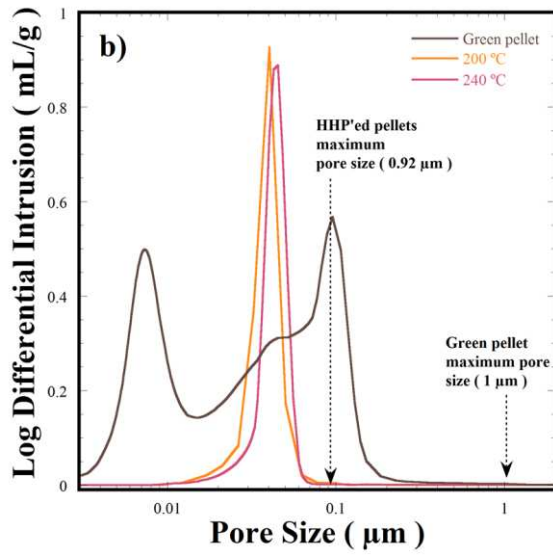


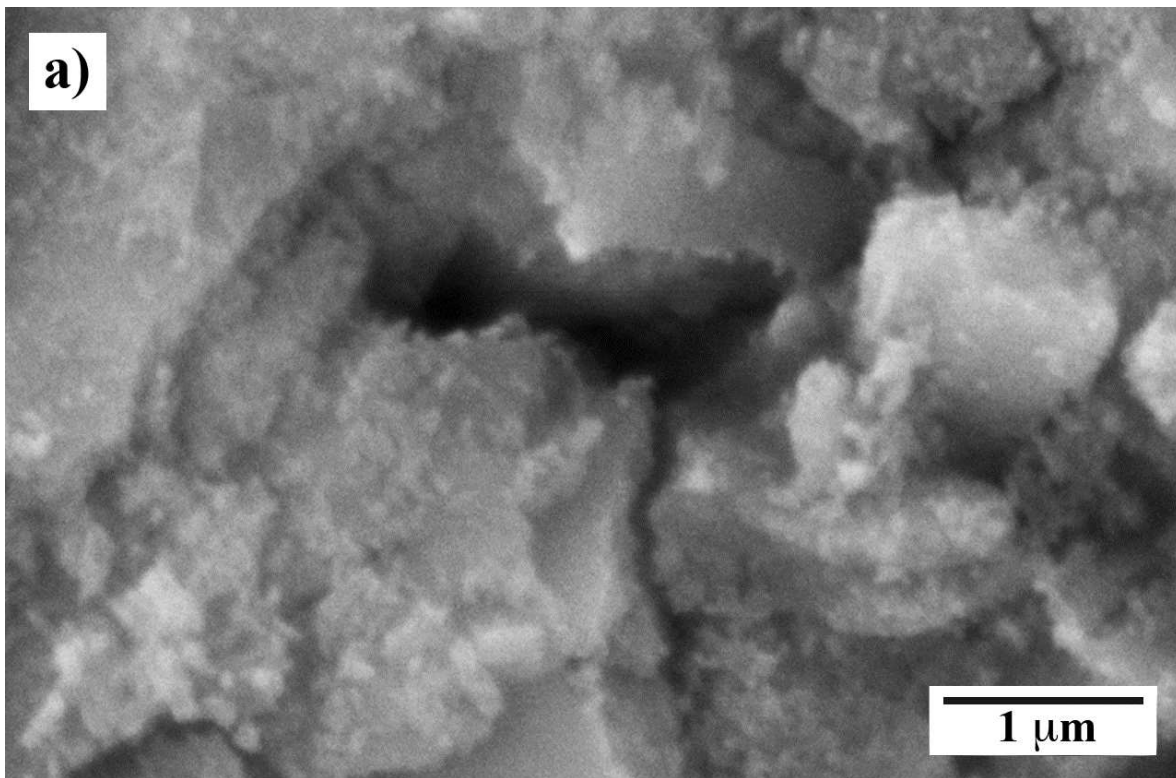
ACC



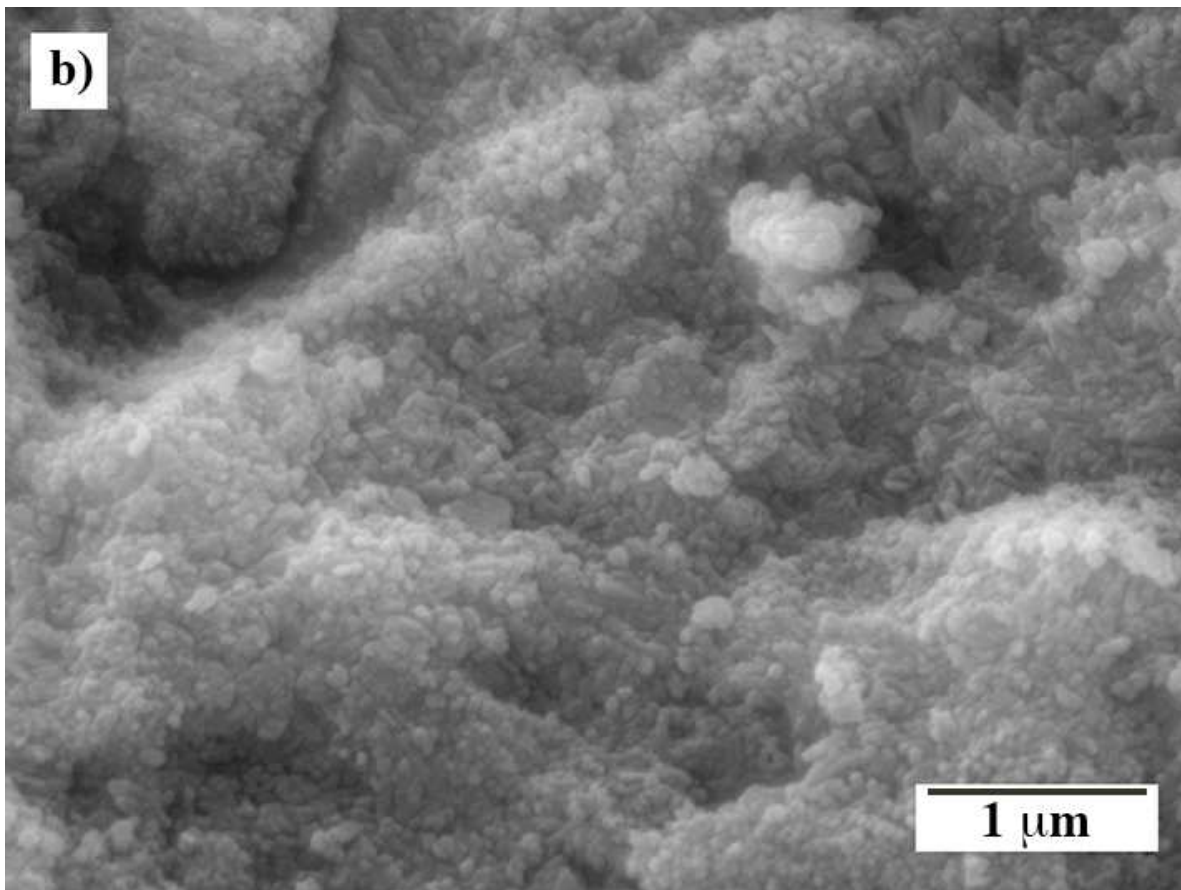




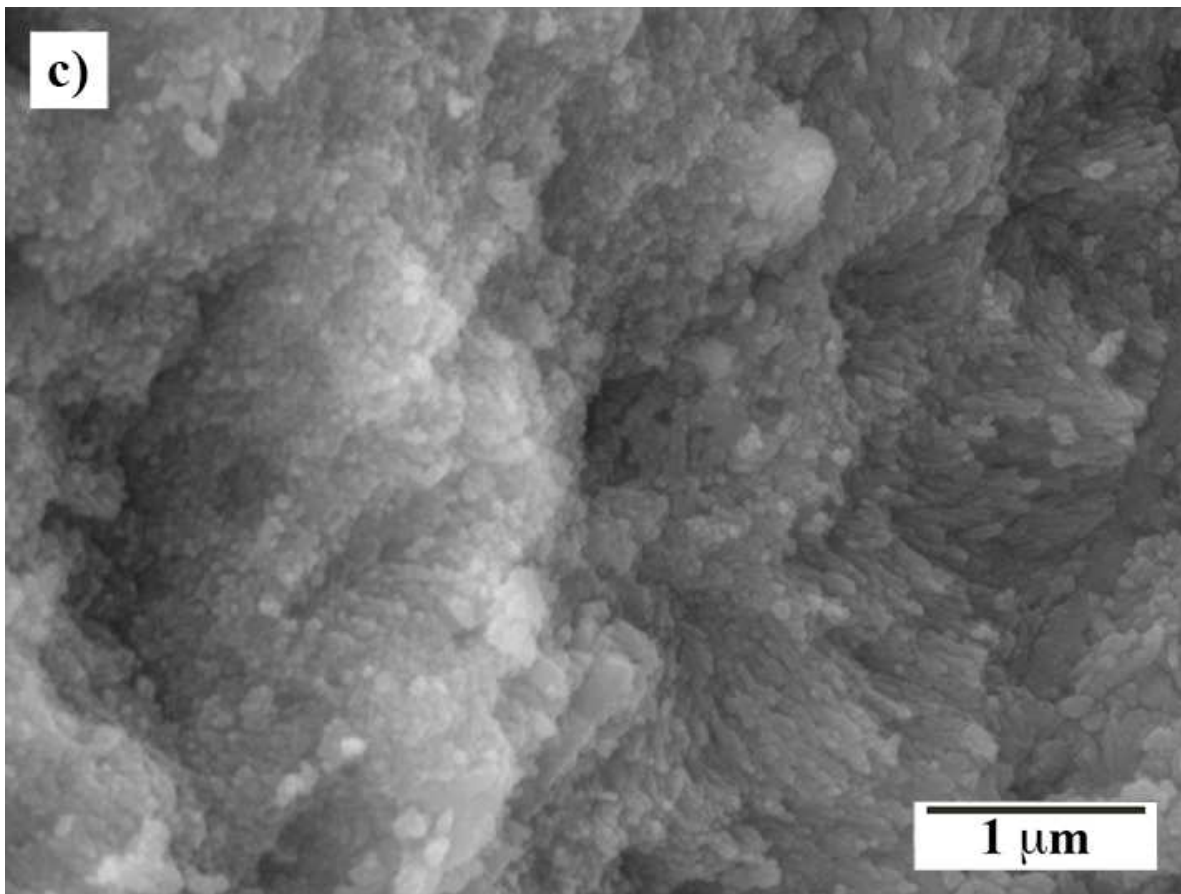




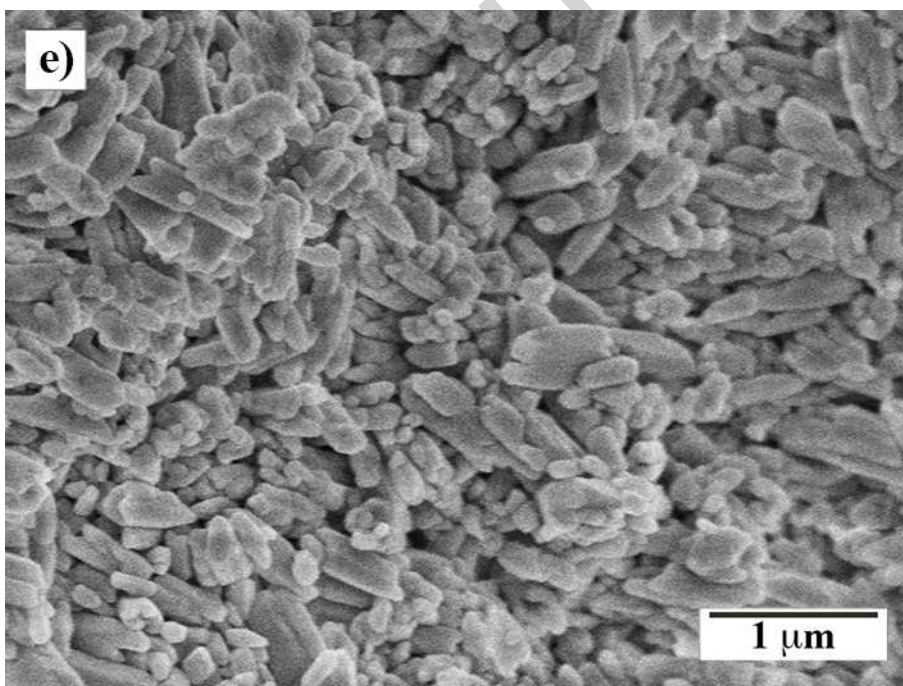
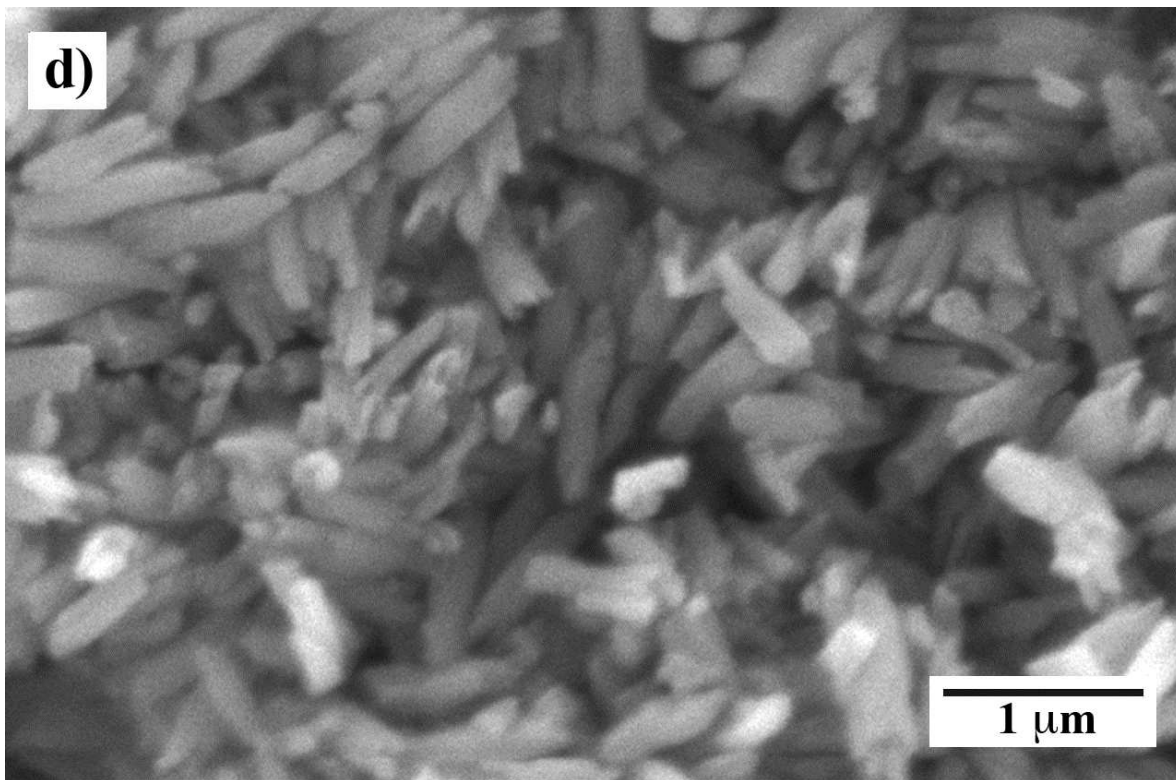
Accepted manuscript

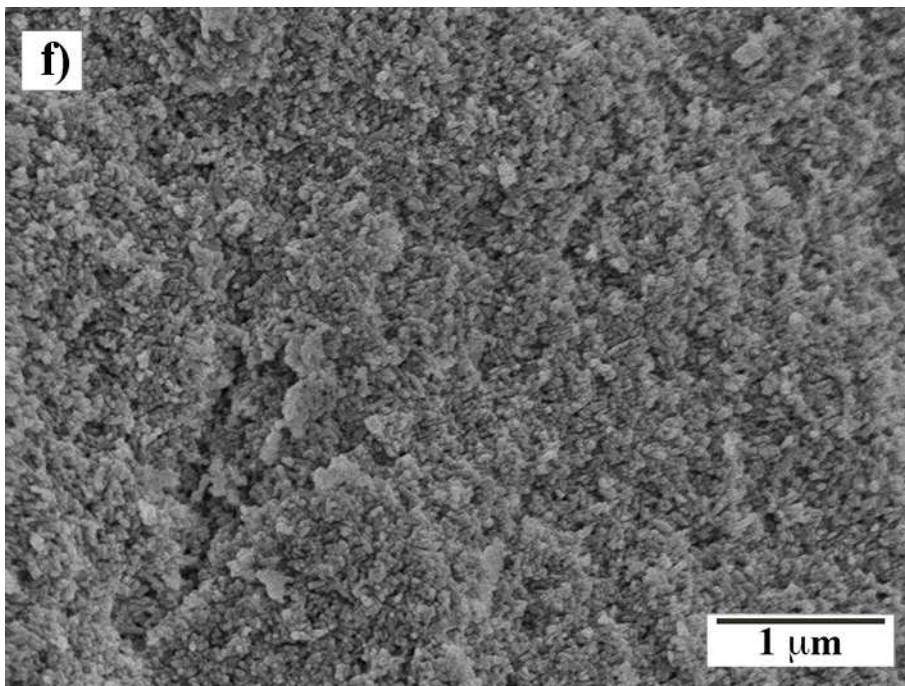


Accepted

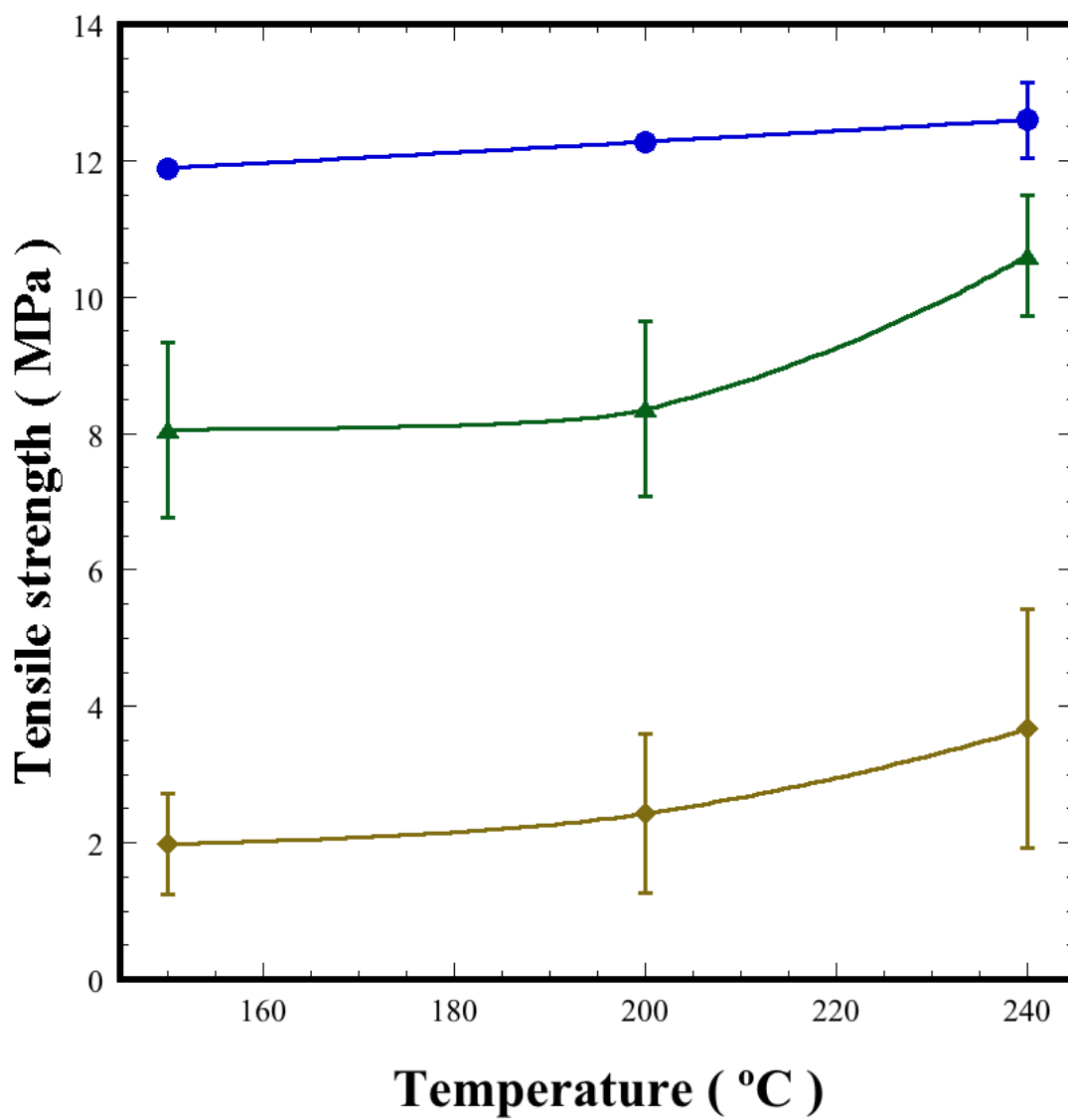


Accepted





Accepted manuscript



ACC